의학박사 학위논문

Development of oxadiazole-based ODZ10117 as a small molecule inhibitor of STAT3 for targeted cancer therapy

표적암치료를 위한 저분자 STAT3 저해제인 옥사디아졸계 ODZ10117 의 개발

2020 년 8 월

서울대학교 대학원

의과학과 의과학전공

이 해 리

A thesis of the Degree of Doctor of Philosophy

표적암치료를 위한 저분자 STAT3 저해제인 옥사디아졸계 ODZ10117 의 개발

Development of oxadiazole-based ODZ10117 as a small molecule inhibitor of STAT3 for targeted cancer therapy

August 2020

The Department of Biomedical Sciences,
Seoul National University
College of Medicine
Haeri Lee

ABSTRACT

Development of oxadiazole-based ODZ10117 as a small molecule inhibitor of STAT3 for targeted cancer therapy

Haeri Lee
The Department of Biomedical Sciences
The Graduate School
Seoul National University

STAT3 is a transcription regulator involved in many intracellular functions, including cell proliferation, differentiation, survival, angiogenesis, and immune response. Persistently activated STAT3 is a promising target for a new class of anticancer drug development and cancer therapy, as it is associated with tumor initiation, progression, malignancy, drug resistance, cancer stem cell properties, and recurrence.

Here, I discovered 3-(2,4-dichloro-phenoxymethyl)-5-trichloromethyl-[1,2,4]oxadiazole (ODZ10117) as a small molecule inhibitor of STAT3 and suggested that it may have an effective therapeutic utility for the STAT3-targeted cancer therapy. ODZ10117 targeted the SH2 domain of STAT3 regardless of other STAT family proteins and upstream regulators of STAT3, leading to inhibition of the tyrosine

phosphorylation and transcriptional activity of STAT3. The inhibitory effect of ODZ10117 on STAT3 was stronger than the known STAT3 inhibitors such as S3I-201, STA-21, and nifuroxazide. Furthermore, I demonstrated the therapeutic efficacy of ODZ10117 by targeting STAT3. ODZ10117 suppressed the cancer cell migration and invasion, induced apoptotic cell death, and reduced tumor growth in both *in vitro* and *in vivo* models of breast cancer and glioblastoma. In addition, ODZ10117 suppressed stem cell properties in glioma stem cells (GSCs).

To confirm these results, I demonstrated two different types of xenograft model. First, I have shown that extended the survival rate and reduced lung metastasis in models of breast cancer. Next, the administration of ODZ10117 showed significant therapeutic efficacy in mouse xenograft models of GSCs. In conclusion, I believe this study provides insight in to a promising therapeutic candidate for cancers by targeting STAT3.

Keywords: ODZ10117, STAT3, targeted therapy, invasion, migration, apoptosis

Student number: 2012-23672

CONTENTS

Abstract i

Contents iii

List of figures iv

List of abbreviations vii

Introduction 1

Materials and methods 8

Results 20

Figures 34

Discussion 74

References 79

Abstract in Korean 86

LIST OF FIGURES

Figure 1. A scheme for identification and optimization of STAT3 inhibitors..... 34
Figure 2. Identification of ODZ17690 as a hit compound by targeting the SH2 domain of STAT3..... 35
Figure 3. Identification of ODZ10117 as a STAT3 inhibitor from the optimization of ODZ17690 37
Figure 4. Molecular docking of ODZ10117 against the SH2 domain of STAT3 38
Figure 5. ODZ10117 inhibits tyrosine phosphorylation of STAT3 in various human cancer cell lines. 41
Figure 6. STAT3 hyperactivation is associated with tumor malignancy and survival in glioblastoma patients 42
Figure 7. ODZ10117 inhibits STAT3 signaling *in vitro*..... 44
Figure 8. ODZ10117 inhibits STAT3 activation in a concentration−and time−dependent manner 46
Figure 9. ODZ10117 has a greater inhibition on STAT3 activation than the known inhibitors 48
Figure 10. ODZ10117 does not affect STAT1 or upstream regulators of STAT3 in breast cancer cells..... 49
Figure 11. ODZ10117 does not affect STAT1 or upstream regulators of STAT3 in glioblastoma cells..... 50
Figure 12. ODZ10117 does not affect other STAT family members or upstream regulators of STAT3 in Hodgkin's

lymphoma cells 51
Figure 13. ODZ10117 decreases cell viability..... 53
Figure 14. ODZ10117 decreases the viability of breast cancer and glioblastoma cells by inducing apoptosis. 54
Figure 15. ODZ10117 induces apoptotic cell death in breast cancer and glioblastoma cells..... 56
Figure 16. ODZ10117 decreases the migration and invasion in breast cancer and glioblastoma cells 57
Figure 17. ODZ10117 decreases the expression of STAT3 target genes associated with migration and invasion 58
Figure 18. ODZ10117 suppressed tumor growth in breast cancer xenograft models 59
Figure 19. ODZ10117 inhibits tumor growth and increases survival in metastatic breast cancer xenograft model..... 61
Figure 20. ODZ10117 inhibits lung metastasis in breast cancer xenograft model 63
Figure 21. Positive correlation between STAT3 and stem cell phenotypes and EMT markers in glioblastoma patients..... 65
Figure 22. STAT3 expression regulates tumorsphere-forming capacity of glioblastoma cells 66
Figure 23. ODZ10117 suppresses STAT3 activation and cancer stem cell markers in GSCs 67
Figure 24. ODZ10117 suppresses stemness features in GSCs 69
Figure 25. ODZ10117 reduces tumor growth in a glioblastoma

xenograft model 71
Figure 26. ODZ10117 reduces tumor growth in a glioblastoma xenograft model 72
Figure 27. A schematic diagram illustrating the proposed action 73

LIST OF ABBREVIATIONS

AG: AG490

Bcl-XL: B-cell lymphoma-extra large

Bcl-2: B-cell lymphoma-2

CSC: Cancer stem cell

EGF: Epidermal growth factor

EMT: Epithelial-mesenchymal transition

FN: Fibronectin

GSC: Glioma stem cell

HER2: Human epidermal growth factor receptor-2

H&E: Hematoxylin and eosin

HTS: Cell-based high-throughput screening

IHC: Immunohistochemistry

IL-6: Interleukin 6

ITGAV: integrinαV

JAK: Janus kinase

Mcl-1: Myeloid cell leukemia-1

NAPA: Napabucasin

NIF: Nifuroxazide

ODZ: Oxadiazole, ODZ10117

qPCR: Quantitative real-time polymerase chain reaction

RMSD: Root-mean-square deviation

SBVS: Structure-based virtual screening

SEM: Standard error of the mean

SH2: Src-homology 2 domain

STAT3: Signal transducer and activator of transcription 3

STA: STA-21

S3I: S3I-201

TNBC: Triple-negative breast cancer

Veh: Vehicle

INTRODUCTION

Signal transducer and activator of transcription 3 (STAT3) is a member of the STAT family consisting of seven proteins in mammals: STAT1, STAT2, STAT3, STAT4, STAT5A, STAT5B, and STAT6 [1, 2]. It was first discovered independently as an acute-phase response factor that selectively binds to DNA in response to interleukin-6 (IL-6) and epidermal growth factor (EGF) [3-5]. STAT3 is a transcription factor that remains in the cytoplasm as an inactivated form and is expressed at a basal level under normal conditions. It can be activated by the phosphorylation of tyrosine 705 residue in response to cytokines, chemokines, and growth factors through receptor- and non-receptor-associated tyrosine kinases [5].

STAT3 signaling cascade is triggered by upstream kinase signals, and undergo phosphorylation, homo-dimerization, translocate in to nuclear, and bind to DNA, leading to target gene expression involved in cell proliferation, survival, angiogenesis, invasion, metastasis, and immunoediting [6-9].

Aberrant activation of STAT3 has been involved in oncogenesis and malignant phenotypes in human cancers [10, 11]. Hyperactivation of STAT3 has been reported in several types of tumors, including head-and neck, brain, breast, liver, lung, kidney, pancreas, prostate, ovary cancer, and multiple myeloma, as well as acute myeloid leukemia (AML) [12-17]. Expression levels of activated STAT3 are positively correlated with poor prognosis in these cancers.

Activated STAT3 can be translocated to the nucleus and regulates the transcription of a variety of genes involved in important biological functions, including cell proliferation, survival, differentiation, angiogenesis, tissue development, and immune responses. However, persistently activated STAT3 signaling is closely associated with oncogenic signaling and is frequently observed in numerous types of cancer cells and tumor tissues of cancer patients [1, 18]. In fact, this signaling is positively correlated with cancer aggressiveness, malignancy, recurrence, drug resistance, and a poor prognosis via promoting the survival, proliferation, invasion, and metastasis of cancer cells and maintaining cancer stem cell (CSC) properties [19–21].

The tumor microenvironment is composed of tumor cells and their surrounding circumstance, including hypoxic condition, blood vessels and extracellular matrix (ECM), as well as stromal cells, immune cells, and inflammatory cells [22, 23]. STAT3 is a key mediator modulating tumor milieu to promote tumor progression, and is a promising target for antitumor immune response [24, 25].

It is well known that tumor cells modify and adapt to their surrounding milieu. Constitutive activation of STAT3 promotes tumor growth through oncogenic signaling pathway, and interacts with tumor cells and their surrounding factors. Constitutive activation of STAT3 promotes tumor growth through oncogenic signaling pathway, and interacts with tumor cells and their surrounding factors. Aberrant activation of STAT3 recruits immune cells and compromises their functions to benefit tumor cells [26].

In the core of tumor tissue, hypoxic stress is generated and therefore induces hypoxia-inducible factors. It is known that STAT3 regulates stability and activity of HIF-1α, inducing expression of cytokines, chemokine, and growth factors to improve cancer development [27, 28]. Also, in response to surrounding tumor cells, stromal cells upregulate their C-X-C motif chemokine ligand 12 (CXCL12) receptors, resulting in enhancing metastatic potential in tumor cells [29]. Additionally, activation of STAT3 promotes polarization of tumor-associated microphages as M2 phenotype and programmed death-ligand 1 (PD-L1) expression as well, which increase tumor progression. Inhibition of STAT3 activation shows anti-tumor activity by suppressing polarization of macrophages [30]. In addition, activation of STAT3 in endothelial cells increases cell adhesion molecule expression and it is important for the tumor metastasis [9, 31].

Tumor cells can evade immune response by regulating their immunological circumstance. Activation of STAT3 is crucial for immune escape of tumor cells, by promoting transforming growth factor-β (TGF-β), vascular endothelial growth factor (VEGF), myeloid-derived suppressor cell (MDSC) expansion and suppressing NK cell function [32]. Using STAT3 inhibitors has shown reduction of immunosuppressive response, therefore upregulating antitumor activity of immune cells

Therefore, targeting persistently activated STAT3 signaling is considered one of the important therapeutic options for cancer treatment.

STAT3 inhibitors or agents can have two major strategies, in which STAT3 activation is inhibited, directly or indirectly. Direct inhibitors block the SH2 domain, DNA-binding domain, and N-terminal domain, which regulate STAT3 activation by blocking phosphorylation, dimerization, nuclear translocation, and DNA binding [33, 34].

The SH2 domain of STAT3 has a binding pocket to phosphorylated tyrosine (pTyr) residue, and formation of STAT3 dimerization involves pTyr interacting with the SH2 domain. Therefore, inhibiting SH2 domain of STAT3 suppresses activation of STAT3 protein. Numerous kinds of small molecule peptides have been developed as STAT3 inhibitors that directly target the SH2 domain of STAT3 by using high-throughput screening and structure-based virtual screening system [9].

Indirect inhibitors target upstream regulators of STAT3 pathway, such as receptor-ligand binding and kinases. However, additional tyrosine kinase mutations or switching to alternative tyrosine kinases can restore STAT3 activation in tumor cells in patients, resulting in acquired resistance to tyrosine kinase inhibitors [9].

Additionally, STAT3 is phosphorylated by various protein kinases in the cytoplasmic region. It is well known that JAK and Src kinases are common STAT3 upstream regulators. JAK and Src kinases inhibitors have various anti-cancer effects such as inducing cancer cell apoptosis and reducing metastasis through decrease in the level of STAT3 phosphorylation [35-39]. Some of these small molecule inhibitors have recently been in clinical trials for chemotherapy for various cancer treatment, and

inflammatory syndromes including rheumatoid arthritis, psoriasis, and inflammatory bowel disease (IBD) [40-43].

Therefore, inhibiting STAT3 activity by targeting STAT3 directly could be a highly beneficial strategy for the successful treatment of cancer.

To date, a number of compounds that inhibit STAT3 phosphorylation and activity have been developed and pre-clinically tested. For example, few non-peptide STAT3 SH2 inhibitors were recently developed to inhibit STAT3 dimerization, including Stattic [44], STA-21 [45], and S3I-201[46]. Several new inhibitors of JAK2, the upstream kinase of STAT3, such as AG490 [47], WP1066 [48] have also been reported.

Breast cancer is the most commonly diagnosed cancer and the second leading cause of cancer mortality in women worldwide. The incidence of breast cancer increases with age and the survival rate of patients generally decreases in case of invasive malignant characteristics [49]. Based on the receptor patterns of genomic expression profiling, breast cancer is classified into four major classes: luminal A, luminal B, human epidermal growth factor receptor-2 (HER2)-positive, and triple-negative breast cancer (TNBC) [50, 51].

Patients with luminal subtypes of breast cancer are typically treated with hormonal and/or HER2-targeted therapy, and the prognosis is generally excellent with a 10-year survival rate of over 95%. In contrast, HER2-positive and TNBC subtypes are invasive breast cancers that are commonly associated with a poorer prognosis, a higher rate of distant recurrence, and the shortest overall survival rate of all breast cancers. These

subtypes of cancer are highly aggressive and have low sensitivity to typical endocrine therapies and the limited number of therapeutic options than other subtypes [52-54].

Glioblastoma is the most frequent and most aggressive occurring type of primary brain tumor in adults. It is positively correlated with a deadly disease with extremely poor prognosis, early clinical deterioration, and high mortality rate. Patients with glioblastoma show a median overall survival of less than 15 months and a 5-year survival rate of less than 5% despite surgical intervention with radiotherapy and chemotherapy [55, 56]. Although extensive studies and advances in modern medicine during past decades have occurred, glioblastoma remains difficult to treat with a very dismal prognosis in patients, because few mechanisms underlying its tumor malignancy have been identified.

Therefore, it is necessary to develop novel therapeutic strategies to improve the survival rate and prognosis of glioblastoma. Recently, the degree of STAT3 activity has emerged as an important biomarker in targeted therapy of cancer patients.

STAT3 is persistently activated in more than 40% of breast cancer patients. Particularly, high level of activated STAT3 is observed in TNBC subtype [52-54] and glioblastoma patients [57, 58], suggesting that STAT3 inhibitors may be an essential strategy for cancer treatment. In this study, I identified 3-(2,4-dichloro-phenoxymethyl)-5-trichloromethyl-(1,2,4) oxadiazole (ODZ10117) as a new STAT3 inhibitor and examined

the anticancer activity of ODZ10117 in both *in vitro* and *in vivo* models of breast cancer and glioblastoma cancer cells.

MATERIALS AND METHODS

1. Structure-based computational database screening

To discover small molecules that target the SH2 domain of STAT3, we prepared a 3D-structure of the SH2 domain by extracting the corresponding region from the X-ray structure of mouse STAT3 (mSTAT3), which was available from the protein data bank (PDB), entry 1BG1 [59]. Multiple sequence alignment between mouse STAT3 (mSTAT3) and human STAT3 (hSTAT3) using the Clustal Omega server (https://www.ebi.ac.uk/Tools/msa/clustalo/, Windows 1.2.2) showed that the template and target sequence share 99.83% sequence identity and the remaining variability occurs in the N-terminal region. Amino acid sequences for mSTAT3 and hSTAT3 were downloaded from the UniProtKB database using the accession numbers P42227 and P40763, respectively. We used the mSTAT3 3D-structure for docking and the structure was prepared at default level using the Protein Preparation Wizard [60] in the Maestro utility of the Schrödinger 2017-4 Suites package.

The chemical databases were obtained from our in-house library with a molecular weight of less than 300 g/mol and each compound was sketched using the ChemDraw Professional 16 software (16.0.1.4) and imported to the Maestro LigPrep module [61]. The default settings of the LigPrep module were used to prepare the ligands. The peptide Pro-pTyr-Leu was obtained from the 1BG1 protein and assigned a grid that covered 5Å

surrounding Pro-pTyr-Leu. The Glide module [62] with the standard precision (SP) docking algorithm was used to further study docking and obtain docking solutions. Fifty docking poses were generated for each ligand and ranked according to Glide docking score. Tighter binding is reflected by a greater negative docking score and vice versa.

We repeated the same procedures to dock the known STAT3 inhibitors, S3I-201 [46] and STA-21 [45] against the SH2 domain of STAT3 for comparison. Figures were generated using the Discovery Studio Client 2018, and Pymol 2.1.0.

2. Cell-based high-throughput screening

To perform cell-based high-throughput screening, we generated MDA-MB-231/STAT3-Luc cells stably expressing both the p21×STAT3-firefly luciferase [63] and pRL-TK Renilla luciferase reporter constructs. Cells were incubated for 24 h in the presence of each compound and the reporter activity was quantified by measuring the relative luciferase units.

The luciferase activity was calculated using the ratio of the activity of firefly luciferase to that of Renilla luciferase. We also generated S2-NP/STAT92E-Luc cells stably expressing both the p10×STAT92E-firefly luciferase and RNA polymerase III Renilla luciferase reporter constructs, and a cell-based luciferase assay was performed as previously described [64].

3. Reagents and antibodies

The known STAT3 inhibitors S3I-201 (SML0330) [46], STA-21 (SML2161) [45], and nifuroxazide (481984) [65], and

the pan-JAK inhibitor AG-490 (T3434) [47] were purchased from Sigma-Aldrich (St. Louis, MO, USA). An inhibitor of STAT3 and cancer stemness, napabucasin (HY-13919) [66] and recombinant human interleukin 6 (IL-6, 200-06) were obtained from MedChem Express (Monmouth Junction, NJ, USA) and PeproTech, respectively. All of the other chemicals used were analytical grade and purchased from Sigma-Aldrich unless otherwise noted.

Antibodies specific for phospho-JAK1 (Tyr1022/1023), JAK1, phospho-JAK2 (Tyr1007/1008), JAK2, phospho-JAK3 (Tyr980/981), phospho-TYK2 (Tyr1054/1055), TYK2, phospho-STAT1 (Tyr701), STAT1, phospho-STAT3 (Tyr705), phospho-STAT5 (Tyr694), phospho-STAT6 (Tyr641), STAT6, phospho-Akt (Ser473), Akt, phospho-Lyn (Tyr507), Lyn, phospho-Src (Tyr416), Src, phospho-ERK1/2 (Thr202/Tyr204), ERK1/2, NESTIN (4760), SOX2 (3579), NANOG (4903), OCT4 (2840), PARP (9542), caspase-3 (9662), and active caspase 3 (9661) were obtained from Cell Signaling Technology (Danvers, MA, USA). Antibodies against fibronectin (ab2413), and integrin αV (ab179475) were obtained from Abcam (Cambridge, MA, USA). Antibodies specific for STAT5 (sc-74442), and GAPDH (AbC-2003) were obtained from Santa Cruz Biotechnology (Santa Cruz, CA, USA), R&D systems (Minneapolis, MN, USA), Novus Biologicals (Centennial, CO, USA), and Abclone (Seoul, Korea), respectively.

4. Cell lines and preparation of primary cell lines

MDA-MB-231, MDA-MB-468 and 4T1 were obtained

from the American Type Culture Collection (Manassas, VA, USA) and maintained in DMEM, EMEM, or Leibovitz's L-15 medium supplemented with 10% fetal bovine serum (FBS) and 1% penicillin/streptomycin (DMEM complete medium; all from GE Healthcare Life Sciences). MDA-MB-231/STAT3-Luc cells were maintained in Leibovitz's L-15 medium supplemented with 10% FBS, 1% penicillin/streptomycin, and 500 μg/mL geneticin.

HDLM-2 and L540 cells were obtained from the German Collection of Microorganisms and Cell Cultures and maintained in RPMI supplemented with 20% FBS and 1% penicillin/streptomycin.

Human glioblastoma cell lines A172 (CRL-1620) and U87 were obtained from ATCC and cells were maintained in DMEM complete medium. GSC lines 19, 84, and 528 were obtained from Dr. Ichiro Nakano (The Ohio State University, Columbus, OH, USA) and maintained in DMEM/F12 (SH30023.01, HyClone) supplemented with 0.04% modified B27 (17504044, Invitrogen, Carlsbad, CA, USA), 1% L-glutamine (25030081, Invitrogen), 20 ng/mL basic fibroblast growth factor (100-18B, PeproTech, Rocky Hill, NJ, USA) and 20 ng/mL epidermal growth factor (GMP100-15, PeproTech).

Human glioblastoma tissue samples were obtained from the patients with glioblastoma who visited the Department of Neurosurgery, Seoul National University College of Medicine. All the patients participating in this study provided informed consent before the surgical procedure at the Seoul National University Hospital. The study was approved by the Institutional Review Board protocols from Seoul National University College of

Medicine (H-0507-509-153) in accordance with the Declaration of Helsinki.

The primary glioblastoma cell lines were prepared from the tumor tissue samples of glioblastoma patients code-named with GBM12 and 14, and maintained in DMEM (SH30243.01, HyClone, Carlsbad, CA, USA) supplemented with 10% FBS (16000044, Gibco, Carlsbad, CA, USA) and 1% penicillin/streptomycin (15070063, Gibco). All the cells were maintained at 37 ℃ in a 5% CO_2 humidified incubator.

5. Western Blot analysis

Whole-cell lysates were prepared using a lysis buffer containing 50 mM Tris-HCl (pH 7.4), 350 mM NaCl, 1% Triton X-100, 0.5% Nonidet P-40, 10% glycerol, 0.1% SDS, 1 mM EDTA, 1 mM EGTA, 1 mM Na3VO4, 1 mM phenylmethylsulphonyl fluoride, and protease and phosphatase inhibitor cocktails (78440, Thermo Scientific, Rockford, IL, USA). Protein samples were separated by SDS-PAGE, transferred to nitrocellulose membrane (Pall Corporation, Port Washington, NY, USA), and performed Western blotting with appropriate antibodies.

6. RNA extraction, cDNA preparation, and quantitative real-time PCR

Total RNA was extracted using TRIzol reagent and cDNA was synthesized using a ReverTra Ace® qPCR RT Kit. Quantitative real-time PCR (qPCR) was performed using a QuantiFast SYBR Green PCR master mix with an Applied

Biosystems 7300 thermocycler.

The primers used in this experiment were *BCL-2* (QT00025011), *BCL-XL* (QT00236712), *MCL-1* (QT00094122), *SURVIVIN* (QT01679664), *MMP-2* (QT00088396), *MMP-9* (QT00040040), *TWIST* (QT00011956), *NESTIN* (QT01015301), *SOX2* (QT00237601), *NANOG* (QT01844808), *OCT4* (QT00210840), and *GAPDH* (QT0007924) were obtained from Qiagen.

Data were analyzed using comparative Ct quantification and each sample was processed in parallel with assays for the housekeeping gene *GAPDH* expression.

7. Cell viability assay

Cells were seeded at 10,000 cells per well in 96-well plates and incubated in culture medium until 70–80% confluence. The cells were further incubated with either vehicle alone or various concentrations of ODZ10117 for 24 h. Cell viability was measured at 450 nm using microplate reader (Molecular Devices, Sunnyvale, USA) after being further incubated for 2–4 h at 37 ℃ following the addition with EZ-CyTox Enhanced Cell Viability Assay Reagent (Daeil Lab Service, Seoul, Korea).

8. Flow Cytometry

To analyze cell cycle and apoptotic cell population, cells were fixed with 70% ice-cold ethanol, washed with PBS, incubated with RNase (50 μg, 10109134001, Sigma Aldrich) at 37 ℃ for 1 h, and stained with propidium iodide (PI, 20 μg, 556463, BD Biosciences, San Jose, CA, USA) at 4 ℃ in the dark. For Annexin

V staining, Annexin V binding buffer (422201, BioLegend, San Diego, CA, USA) containing fluorescein isothiocyanate (FITC) conjugated with anti-Annexin V antibody (640906, 1:50 dilution, BioLegend) was used as manufacturer's protocol. Stained cells were counted with flow cytometry using the BD LSRFortessa^{TM} cell analyzer (BD Biosciences).

9. Immunohistochemistry

Tissue samples were fixed with 4% paraformaldehyde in 0.5 M phosphate buffer and embedded in paraffin. The paraffin blocks were cut in 4-μm-thick sections, mounted on glass slides, dewaxed, rehydrated with grade ethanol, and stained with hematoxylin and eosin (H&E, HT100132, Sigma Aldrich and S3309, Dako, Carpinteria, CA, USA).

To perform immunohistochemical analysis, rehydrated slide sections were unmasked with 10 mM sodium citrate buffer, quenched endogenous peroxidase for 20 min in 3% hydrogen peroxide, blocked for 30 min in PBS containing 10% goat serum, and incubated at 4 ℃ for overnight with appropriate primary antibodies with 1:100 dilution. The sections were incubated with biotinylated secondary antibody (anti-rabbit for BA-1000, anti-mouse for BA-9200 and anti-goat for BA-5000, Vector Labs, Burlingame, CA, USA) compatible with the primary antibody for 30 min, subsequently incubated with streptavidin-HRP (550946, BD Pharmingen, San Jose, CA, USA) for 40 min, and stained with 3,3-diaminobenzidine (D22187, Invitrogen). Digital images were obtained using the LAS Microscope Software (Leica Microsystems, Wetzlar, Germany).

10. Immunofluorescence Staining

Cells grown in lysine-coated 24-well plates were fixed for 45 min at room temperature in 3% paraformaldehyde in PBS and permeabilized for 10 min with 0.1% Triton X-100 in PBS. The plates were blocked for 20 min with 3% BSA in PBS and incubated with tyrosine phosphorylated STAT3 (pY705-STAT3) antibody at 4 ° C overnight. After washing with PBS, the dishes were incubated with fluorescein isothiocyanate (FITC)-conjugated secondary antibody at room temperature for 2 h. Nuclei were counterstained with 4′,6-diamidino-2-phenylindole (DAPI, D8417, Sigma-Aldrich) and images were captured using a Zeiss Axiovert 200 inverted fluorescence microscope (Oberkochen, Germany) with an LSM 510 META system (ZEN 2011). pY705-STAT3 antibody was used at 1:200 dilution.

11. Wound healing and invasion assays

To conduct wound healing assay, cells were seeded into 12-well plates and then incubated over 90% confluence. The plate was scratched with pipette tips and washed with PBS. Cells were incubated for 24 h with fresh DMEM complete medium containing either vehicle alone or ODZ10117 for 24 h. Digital images were obtained using the Leica Application Suite (LAS) Microscope Software (Leica Microsystems).

Invasion assay was conducted using a Boyden chamber system (Neuro Probe, Gaithersburg, MD, USA). Growth factor reduced Matrigel (354230, BD Matrigel™, BD Biosciences) was diluted with serum free media with ratio of 1:3. Diluted Matrigel

was transferred into 24-transwell (BD 24-well insert, 8 μm pore transparent PET filter) and incubated at least for 4 to 5 h for gelling at 37 ℃. Cells in 100 μL DMEM containing 1% FBS were seeded in the upper chamber and incubated for 24 h in the presence of either vehicle alone or ODZ10117. The lower chamber was filled with 500 μL of 10% DMEM containing fibronectin (5 μg/mL, ECM001, Sigma-Aldrich). Matrigel containing upper chamber was rinsed with PBS, fixed, stained with Diff-Quik solution (Sysmex Corporation, Kobe, Japan), and subsequently rinsed with distilled water.

The migrated cells were captured using the LAS Microscope Software (Leica Microsystems).

12. Limiting dilution and sphere-forming assays

Sequentially decreasing numbers of GSCs were seeded into 96-well plates and incubated for 2 weeks. Colonies were counted and photographed with microscope (Olympus, Tokyo, Japan). Stem cell frequency was calculated using the extreme limiting dilution analysis (ELDA) software [67].

To determine sphere-forming capacity, dissociated single cells were seeded at 10,000 cells per well into 24-well plates and incubated for 5 days in the presence of vehicle alone, ODZ10117, or each of the known STAT3 inhibitors. Sphere formation was captured using a microscope (Olympus).

13. *In vivo* xenograft models

An orthotopic xenograft model was generated by the introduction of MDA-MB-231 cells (1×10^6 cells in 50 μL HBSS

containing growth factor reduced 25% Matrigel) into the right fourth mammary fat pad of 6-week-old female BALB/c nude mice under anesthesia using a 30-gauge insulin needle (n = 6). Intraperitoneal treatment with vehicle control (5% EtOH, 40% PEG400, 55% DW) or ODZ10117 (1 mg/kg or 10 mg/kg) was initiated at 17 days post-tumor cell inoculation, followed by injecting 5 times per week for 23 days.

To generate syngeneic xenograft model, 4T1-Luc cells (5×10^5 cells in 50 μL HBSS containing growth factor reduced 25% Matrigel) were injected into the right fourth mammary fat pad of 6-week-old female BALB/c mice using a 30-gauge insulin needle under anesthesia. After 11 days, mice were randomly divided into three groups (n = 10) and vehicle (DMSO and corn oil = 1:9) alone, ODZ10117 (1 or 10 mg/kg), or napabucasin (10 mg/kg) was intraperitoneally administered 5 times per week for 3 weeks. At the end of the experiment, the lungs were resected and fixed in Bouin's solution and the visible metastatic nodules in the lungs were quantified.

To generate an orthotopic xenograft model, GSC528 cells (5×10^4 cells in 3 μL of PBS) were stereotactically injected into the right striatum of 6-week-old BALB/c nu/nu nude mice (coordinates relative to the bregma: medial-lateral +2 mm, and dorsal-ventral -3 mm). After 14 days, mice were randomly divided into three groups (n = 7) receiving an intraperitoneally injection of ODZ10117 (0.1 mg/kg or 1 mg/kg) in solvent (DMSO:corn oil, 1:9) or equal volume of solvent only (control). Mice were injected six times per week and body weight was measured every day. Animals were monitored daily after

treatment for the manifestation of any pathological signs. To compare the tumor histology, all mice were sacrificed at the same time when one mouse initially exhibited neurological symptoms.

All experiments in the present studies involving animals were approved by the IACUC at the Korea University and Seoul National University College of Medicine, and were performed in accordance with government and institutional guidelines and regulations.

14. Bioluminescence imaging

Mice were intraperitoneally administered firefly D-Luciferin potassium salt at a dose of 150 mg/kg body weight in Dulbecco's PBS. Bioluminescence images were obtained with the IVIS Lumina system under anesthesia with 2% isoflurane. Analysis was performed using Living Image® Software (Windows 4.7.3) by measuring the photon flux (photons/s/cm2/sr) for approximately 1 h using a region of interest manually drawn over the body of the mouse.

15. Statistics

Each experiment was performed independently at least twice, and the results are represented as the mean ± standard error of mean (SEM), unless otherwise indicated. Statistical analyses were performed with GraphPad Prism 5.0 (GraphPad Software, San Diego, CA, USA).

The significance was determined using the two-tailed Student's *t*-test. Survival analysis was conducted by the Kaplan-Meier method with the log-rank test. A *p*-value of less

than 0.05 was considered statistically significant for all analyses.

RESULTS

Identification of ODZ17690 as a hit compound by targeting the SH2 domain of STAT3

To identify small-molecule inhibitors that target STAT3, I performed combined screening assays in combination with structure-based computational database screening and cell-based high-throughput screening using our in-house compound library with molecular weight less than 300 g/mol (Figure 1).

For virtual screening, I used the 3D structure of the SH2 domain of STAT3 (PDB ID: 1BG1) and selected the coordinate from the complex structure of STAT3-DNA (PDB: 1BG1) [59]. The docking was performed using the Glide module [62] with the SP docking algorithm. I also performed cell-based high-throughput screening using the luciferase reporter constructed MDA-MB-231/STAT3-Luc cells.

Therefore, I identified 5-*tert*-butyl-3-(3-nitro-phenoxymethyl)-(1,2,4)oxadiazole (ODZ17690) as a hit compound, which showed the lowest Glide docking score at -3.37 kcal/mol (Figure 2A). The nitro group of ODZ17690 docked in the polar environment of the SH2 domain and interacted with Lys591 and Arg609 via a salt bridge and attractive charge interaction. Hydrogen bond interactions were shown by the nitro group and oxadiazole with the Ser611 and Glu638 residues, respectively. Pro639 was involved in a pi-alkyl interaction with the phenyl group of ODZ17690. Glu612, Ser613, Thr620, Trp623, Lys626, and Gln635 were involved in van der Waals

interactions with ODZ17690 (Figure 2B). ODZ17690 inhibited the transcriptional activity of STAT3 in MDA-MB-231/STAT3-Luc cells without affecting their viability (Figure 2C).

Discovery of ODZ10117 as a STAT3 Inhibitor

To optimize pharmacological activity, we synthesized 144 compounds that were modified based on the core structure of ODZ17690 and identified 3-(2,4-dichloro-phenoxymethyl)-5-trichloromethyl-[1,2,4]oxadiazole (ODZ10117). I finally selected ODZ10117 from the results of combined screening assays and immunoblot analyses (Figure 3A and B).

The molecular docking results showed that ODZ10117 snugly fits into the phospho-tyrosine binding pocket on the SH2 domain of STAT3 with a docking score of -6.17 kcal/mol and participated in many interactions with surrounding residues of the SH2 domain. ODZ10117 mainly showed hydrogen bond interactions with Lys591, Arg609, and Ser611. It also displayed an amide-pi interaction with Val637. Chlorine from the tri-chloromethyl group showed a halogen bond interaction with Glu612. Other interactions were mainly of the van der Waals type. The meta Cl position in the dichloro-benzene moiety of ODZ10117 was located at the position corresponding to the phosphate-moiety of phospho-tyrosine, clarifying the role of the atom (Figure 4A-C and E).

To perform a comparative analysis of ODZ10117 with tripeptide Pro-pTyr-Leu as a substrate and reference compounds S3I-201 and STA-21 as a STAT3 inhibitor by

binding to the site of SH2 dimerization [45, 46], I created superimposed orientations of the selected ligand postures (Figure 4D).

First of all, I docked a tripeptide in the SH2 domain and analyzed the docking orientations of the tripeptide. The results suggest that the best docking orientation of the tripeptide had a 1. 97Å root-mean-square deviation (RMSD) with the native tripeptide and docking score of -6.43 kcal/mol. The tripeptide participated in several interactions with the surrounding SH2 domain residues. The phospho-tyrosine of the tripeptide showed pi-cation and salt bridge interactions with the crucial Lys591. Pro639 showed a pi-alkyl interaction with the pTyr. The phosphate group showed several hydrogen bond interactions with the Lys591, Arg609, Ser611, the main chain of Glu612 and Ser613. Also, Arg609 showed an attractive charge type interaction with the phosphate O. Leu706 of the tripeptide showed hydrogen bond interactions with the Ser636 and Glu638, and an alkyl-alkyl interaction with the side chain of Lys626. The strong network of interaction patterns led to the higher docking score of the tripeptide inside the SH2 domain of STAT3 (Figure 4F).

The S3I-201 was docked inside the SH2 domain with a Glide docking score of -5.87 kcal/mol. The carboxylic acid group of S3I-201 was bound to Arg609, Ser611, Glu612, and Ser613 via hydrogen bond interactions. The hydroxyl group on the phenyl ring also hydrogen bonded with Arg609. Another hydrogen bond was observed between the Glu638 and sulphonyl O of S3I-201. Lys626 showed an alkyl interaction with the 4-methylphenyl,

and Pro639 displayed a pi-alkyl interaction with the 4-carboxyphenyl moiety. Thr620, Trp623, Gln635, Ser636, and Val637 interacted through van der Waals interactions with S3I-201 (Figure 4G).

The STA-21 bound with a Glide docking score of -3.58 kcal/mol, and showed two hydrogen bond interactions with the crucial Lys591. Amide-pi and alkyl interactions were observed between STA-21 and Val637 and Pro639. Pi-donor hydrogen bond interactions were observed between the pi-cloud of the fused ring system of STA-21 and main chain NH of Ser636. This smaller ligand size led to a minimal interaction network with the surrounding SH2 domain of STAT3 (Figure 4H).

These results indicate that ODZ10117 is more effective than ODZ17690, and the binding of ODZ10117 to the SH domain of STAT3 was comparable to that of the tripeptide and lower than those for S3I-201 and STA-21, indicating higher affinity.

I further observed that ODZ10117 effectively inhibited the level of tyrosine phosphorylated STAT3 in various cancer cell lines such as Hodgkin's lymphoma cancer cells (L-540 and HDLM-2), leukemia cell line (K562, KCL22), breast cancer cell line (ZR-75-1, 4T1, MDA-MB-231, MDA-MB-468), ovarian cancer cell line (SKOV3), pancreatic cancer cell line (PANC-1), human alveolar basal epithelial cells(A549), lung cancer cell line (NCI-460), colon cancer cell line (HCT116, SW620), gastric cancer cell line (MKN-45), squamous carcinoma cell lines (A431), human melanoma cell line (A375, SK-MEL-146), hepatocellular carcinoma (HepG2, Huh7), glioblastoma cell line (A172, U87MG, U373MG) and neuroblastoma cell line (SH-

SY5Y) which are persistently express a high level of activated STAT3 (Figure 5A).

In addition, I observed that the compound suppress STAT3 activation in cell lines with low STAT3 expressions such as myeloma (RPMI8226, U266), lymphoma (U937), human leukemia cell line(HL-60), cervical cancer cell line (HeLa), breast cancer cell line (MCF-7) and glioblastoma (U251MG) activated by IL-6-stimulation (Figure 5B).

STAT3 Hyperactivation Increases Tumor Malignancy and Decreases Survival in Glioblastoma Patients

Glioblastoma represents various features of tumor malignancy and high resistance to current therapeutic approaches such as surgery combined with radiochemotherapy [55, 56, 58]. To investigate the negative roles of STAT3 in brain tumors, we analyzed the database of The Cancer Genomic Atlas (TCGA) Research Network. The mRNA level of STAT3 was positively correlated with the grade of brain tumor (Figure 6A). In addition, the survival rate was shorter with the higher mRNA level of STAT3 in patients with glioblastoma (Figure 6B).

I further analyzed the level of active STAT3 (phosphorylated at tyrosine 705 residue) in glioblastoma and primary glioblastoma cell lines. In particular, the level of active STAT3 was relatively higher in five patients, and these patients had a shorter survival rate than the remaining patient code-named with GBM12 (Figure 6C). The overall mean survival rates were 433 ± 276 days in the six patients, 340 ± 173 days in patients with higher levels of active STAT3, and 899 days in patients

called GBM12, with lower levels of active STAT3. These results indicate that STAT3 is closely correlated with tumor malignancy and decreases survival in glioblastoma patients.

ODZ10117 inhibits STAT3 signaling *in vitro*

According to the STAT3 signaling cascades, tyrosine phosphorylated STAT3 sequentially results in the homodimerization, nuclear translocation, and transcriptional activation of STAT3, inducing the expression of numerous target genes by binding to specific DNA sequences [68].

The binding of ODZ10117 to the SH2 domain of STAT3 is thought to result in the breakdown of these sequential cascades. ODZ10117 decreased the nuclear translocation of STAT3 (Figure 7A), and inhibited the transcriptional activity of STAT3 in a concentration-dependent manner with an IC_{50} value of 7.5 μM (Figure 7B). These results clearly indicate that ODZ10117 is an effective STAT3 inhibitor

ODZ10117 has a greater inhibition on STAT3 activation than the known inhibitors

I further verified whether ODZ10117 can inhibit tyrosine phosphorylation of STAT3 in breast cancer and glioblastoma cells. The concentration- and time- dependent results showed that ODZ10117 effectively decreased the level of tyrosine-phosphorylated STAT3 following incubation for 4 h over 20 μM (Figure 8A) or over 2 h at 40 μM (Figure 8B).

In addition, I determined the inhibitory activity of ODZ10117 on tyrosine-phosphorylated STAT3 in comparison with the

known STAT3 inhibitors S3I-201 [46], STA-21 [45], and nifuroxazide [65], and pan-JAK inhibitor AG-490 [47]. The inhibitory effect of ODZ10117 on tyrosine-phosphorylated STAT3 was greater than the known inhibitors in breast cancer and glioblastoma cells that are persistently activated STAT3 activation (Figure 9).

The above-mentioned results indicate that ODZ10117 is an effective STAT3 inhibitor that directly targets the SH2 domain of STAT3, and has a greater inhibitory efficacy than other known inhibitors such as S3I-201, STA-21, nifuroxazide, and AG-490.

ODZ10117 does not affect other STAT family proteins and upstream regulators of STAT3

The mammalian STAT family shares structural similarities and the family proteins can be activated by several upstream regulators including mainly receptor and non-receptor tyrosine kinases [69]. To determine the specificity of ODZ10117 for STAT3, I verified whether ODZ10117 affects other STAT family proteins and upstream regulators of STAT3.

Although ODZ10117 inhibited the tyrosine phosphorylation of STAT3, it did not affect other STAT family proteins, including STAT1 and STAT5 in breast cancer or glioblastoma cells. Next, I evaluated the JAK family of tyrosine kinases, which are direct upstream regulators of STAT family proteins. ODZ10117 did not significantly inhibit the JAK family of tyrosine kinases, including JAK1, JAK2, JAK3 and TYK in breast cancer and glioblastoma cells. ODZ10117 also did not significantly affect other upstream regulators of STAT3, including serine/threonine protein kinase

Akt, the Src family tyrosine kinases Src and Lyn, and MAP kinases ERK1/2. The pan-JAK inhibitor AG-490 (30) effectively inhibited the activation of various JAK, STAT, and Src family proteins (Figure 10 and Figure 11).

Frankly, I did not observe inhibition of STAT5 in both breast cancer and glioblastoma cells. Therefore, I determined to use Hodgkin lymphoma-derived cell lines which are reported to express high levels of constitutively activated STAT1, STAT3, STAT5, and STAT6. As expected, ODZ10117 did not affect STAT1, STAT5, and STAT6 as well as other upstream regulators of STAT3 signaling pathway (Figure 12).

Interestingly, although the effect was cell line-dependent, other STAT3 inhibitors, including S3I-201, STA-21, nifuroxazide, and napabucasin inhibited the tyrosine phosphorylation of various STAT and JAK family proteins, indicating that these compounds are not STAT3-specific inhibitors. Collectively, these results indicate that ODZ10117 is a novel STAT3-specific inhibitor.

ODZ10117 decreases cell viability by inducing apoptosis

Persistently activated STAT3 is associated with excessive cell proliferation and survival in cancer cells [19, 21], indicating that targeting STAT3 can decrease these properties of cancer cells. ODZ10117 treatment decreased the viability of breast cancer and glioblastoma cells in a concentration-dependent manner (Figure 13A and B).

To determine whether the decreased viability of breast cancer and glioblastoma cells by ODZ10117 resulted from

apoptotic cell death, we performed FACS analyses, followed by staining with propidium iodide (PI) and annexin V in each cell line. The population of early apoptotic cell death was increased more than two or fourfold by ODZ10117 compared to that in the vehicle-treated control group (Figure 14A and B).

In addition, ODZ10117 treatment increased the fragmentation of both PARP and caspase-3 (Figure 15A and B) and downregulated the mRNA and protein levels of anti-apoptotic genes such *BCL-2, BCL-xL, MCL-1,* and *BIRC5(SURVIVIN)* (Figure 15C and D), which are regulated by STAT3. These results indicate that ODZ10117 decreased the survival of breast cancer cells by inducing apoptotic cell death via activation of apoptotic proteins and inhibition of anti-apoptotic gene expression.

ODZ10117 reduces the migration and invasion

The migration and invasion of cancer cells into the bloodstream and surrounding tissues are critical steps in cancer metastasis, and the transcription of many target genes associated with these processes is regulated by STAT3 [70]. Therefore, I performed *in vitro* wound healing and Matrigel invasion assays to determine whether ODZ10117 affects the migration and invasion of breast cancer and glioblastoma cells. The results of wound healing assay revealed that the migration of breast cancer and glioblastoma cells was regulated by STAT3, which was decreased in the presence of ODZ10117 compared to the vehicle-treated control group (Figure 16A and B).

Next, I conducted in vitro Matrigel invasion assay to

determine the effect of ODZ10117 in the invasiveness of breast cancer and glioblastoma cells. The lower chamber was filled with culture medium containing 5 ng/mL fibronectin, and primary glioblastoma cells were maintained in the upper chamber for 24 h. The inhibition of STAT3 activity by ODZ10117 decreased the invasiveness of cancer cells compared to the vehicle-treated control group (Figure 16C and D).

In addition, the mRNA levels of *MMP-2 MMP-9, FN, ITGAV, VIMENTIN*, and *TWIST* were effectively suppressed by ODZ10117 treatment compared to those in the vehicle-treated control group (Figure 17A and B). These results suggest that ODZ10117 may suppress cancer metastasis by inhibiting the expression of target genes associated with STAT3-dependent migration and invasion in breast cancer and glioblastoma cells.

ODZ10117 suppresses tumor growth in breast cancer xenografts

Targeting STAT3 is a promising therapeutic strategy in many types of cancer patients. Therefore, I further investigated whether ODZ10117 suppresses tumor growth and metastasis in *in vivo* breast cancer xenograft models. To evaluate the *in vivo* pharmacological activity of ODZ10117, I generated an orthotopic breast cancer xenograft model by injecting MDA-MB-231 cells into the right fourth mammary fat pad of BALB/c mice. At 17 days after inoculation, the tumor bearing mice were intraperitoneally injected with vehicle alone or ODZ10117 (1 mg/kg or 10 mg/kg) 5 times a week for 23 days. The administration of ODZ10117 suppressed the tumor growth compared with the vehicle-treated group (Figure 18A–D),

without affecting the body weight.

ODZ10117 suppresses tumor growth and lung metastasis in breast cancer xenograft

To demonstrate tumor metastasis model, I generated syngeneic xenograft model of spontaneous breast cancer metastasis by injecting 4T1 cells carrying the luciferase gene into the right fourth mammary fat pad of BALB/c mice. At 11 days after inoculation, the tumor-bearing mice were intraperitoneally injected with vehicle alone, ODZ10117 (1 mg/kg or 10 mg/kg), or napabucasin (10 mg/kg) 5 times a week for 3 weeks. The administration of ODZ10117 significantly reduced the progression of primary tumor growth compared with the vehicle-treated group (Figure 19A–C), and showed an excellent extension of median survival rates, which increased from 12 days to 20 days and 21 days, respectively (Figure 19D), without affecting the body weight. Additionally, ODZ10117 treatment reduced lung metastasis of tumor cells with tumor nodules in the lungs (Figure 20 A and B). However, napaubcasin did not demonstrate significant suppression of tumor growth and metastasis, and the median survival rate was 16 days.

Collectively, the results of *in vivo* xenografts models indicate that ODZ10117 exerted effective anticancer activity that suppressed tumor growth and metastasis, leading to the increased survival rate of the mice.

ODZ10117 decreases stem cell properties by inhibiting STAT3 in glioblastoma stem cells

Cancer stem cell (CSC) properties and metastatic capabilities are implicated with tumor malignancy, recurrence and drug resistance in various types of cancer, which are closely associated with STAT3 signaling in the inflammatory tumor microenvironment [71]. To investigate the roles of STAT3 on CSC properties and metastatic capabilities in glioblastoma patients, we analyzed the database of TCGA Research Network. The data revealed that the mRNA level of STAT3 was positively correlated with stem cell-related genes such as *CD133, NESTIN,* and *SOX2* and mesenchymal (MES)-associated genes such as *FN* and *ITGAV* (Figure 21A). Glioblastoma is classified into four subtypes according to the gene expression pattern: proneural (PN), neural (N), classical (CL), and MES [72]. Analyses of the TCGA datasets revealed that the mRNA levels of stem cell-related and MES-associated genes were significantly elevated in all subtypes of glioblastoma patients compared to normal brain tissue (Figure 21B).

Based on the recent studies, the levels of active STAT3 and stem cell markers were positively correlated with the survival rate. To verify this, we determined the tumorsphere-forming capacity of primary glioblastoma cell lines from GBM12 and GBM14. The increase in the size of tumorsphere was of greater magnitude in GBM14 cells than GBM12 cells (Figure 22A), and in GBM14 cells was decreased by the silencing of STAT3 (Figure 22B).

Patient-derived glioma stem cell (GSC) lines have been established from patients with high-grade glioma [73]. The levels of active STAT3 and total STAT3 were highly upregulated

in GSCs, particularly in GSC84 and GSC528 cells, compared to GSC19 cells (Figure 23A). ODZ10117 decreased the level of active STAT3 in the cell lines in a concentration-dependent manner (Figure 23B), with comparable or greater efficacy than S3I-201, STA-21, nifuroxazide, napabucasin, and AG-490 in GSC528 cells (Figure 23C).

The capability of self-renewal is a critical property of CSCs, and the properties of CSCs are mainly determined by their ability to form tumorspheres and by their expression of stem cell markers. According to the tumorsphere forming ability *in vitro*, ODZ10117 reduced the ability of GSC528 cells with comparable to vehicle (Figure 24A). ODZ10117 decreased the mRNA and protein levels of CSC markers such as *NESTIN, SOX2, NANOG, OCT4*, and *CD133* in GSC528 cells (Figure 24B). In addition, ODZ10117 decreased the viability of both GSCs in a concentration-dependent manner (Figure 24C). These results indicate that the STAT3 activity and stem cell properties of GSCs are closely correlated, and ODZ10117 is a potent inhibitor of STAT3 and stemness in glioblastoma and GSCs.

ODZ10117 reduces tumor growth and increases survival in glioblastoma xenograft models

This study suggests that STAT3 targeting may be a promising therapeutic strategy in patients with glioblastoma. Therefore, I investigated whether ODZ10117 could suppress tumor growth in *in vivo* glioblastoma xenograft models. To determine the *in vivo* pharmacological activity, we generated an orthotopic glioblastoma xenograft model by intracranial injection

of GSC528 cells into nude mice. We treated the tumor-bearing mice with vehicle (DMSO:corn oil, 1:9) alone or ODZ10117 (0.1 or 1 mg/kg, daily, intraperitoneal injection) 2 weeks later. ODZ10117 reduces tumor growth without significantly affecting the body weight compared to the vehicle-treated control group (Figure 25A and B).

In addition, ODZ10117 administration increased the median survival rate from 64.5 to 107.0 and 114.0 days, respectively (Figure 26A). When the vehicle-treated control mice exhibited neurological symptoms, the vehicle- and ODZ10117-treated mice were simultaneously euthanized and their tumor tissues were compared. The administration of ODZ10117 dramatically decreased the tumor population and the levels of active STAT3, CSC markers such as NESTIN and SOX2, and mesenchymal-associated genes FN and ITGAV. (Figure 26B).

These results indicate that ODZ10117 suppressed tumor growth and GSC maintenance in glioblastoma xenograft models, which increased the survival rate of the mice, suggesting ODZ10117 to be a promising therapeutic candidate for glioblastoma. In conclusion, the present study has shown that ODZ10117 may be a useful candidate for the STAT3-targeted cancer therapy in glioblastoma. ODZ10117 effectively inhibited tyrosine phosphorylation and nuclear translocation of STAT3, resulting in effective anti-tumor activity in both in vitro and in vivo xenograft models of GSCs.

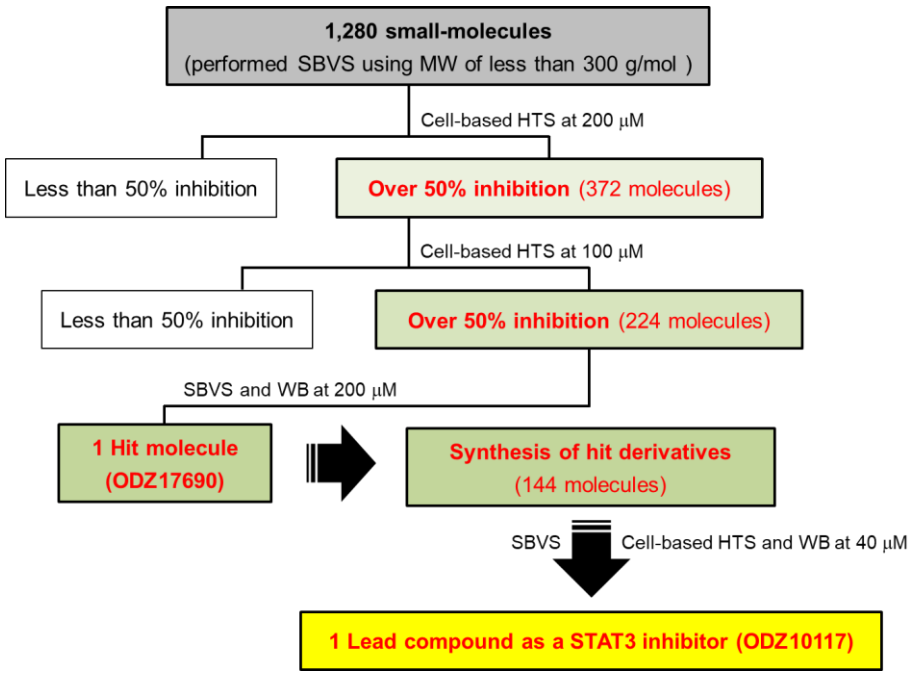

Figure 1. A scheme for identification and optimization of STAT3 inhibitors.

ODZ10117 was identified as a lead compound of STAT3 inhibitor from the 144 derivatives of ODZ17690. ODZ17690 was identified as a hit molecule from the in-house library with a molecular weight of less than 300 g/mol (1,280 compounds) using the structure-based virtual screening (SBVS), cell-based high-throughput screening (HTS), and Western blotting (WB).

A

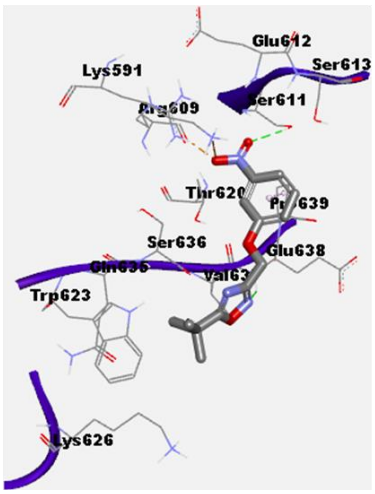

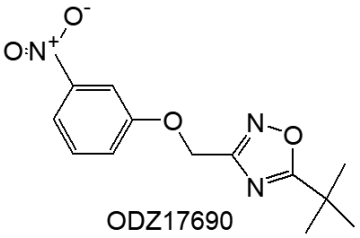

ODZ17690

($C_{13}H_{15}N_3O_4$, MW = 277.28)

B

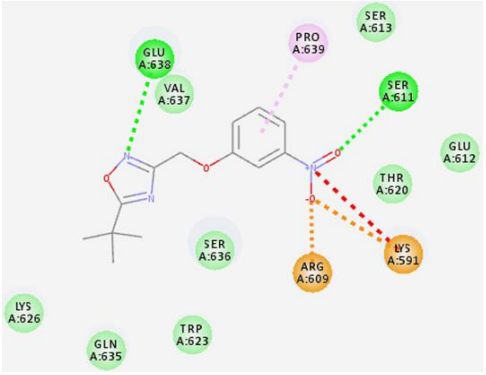

C

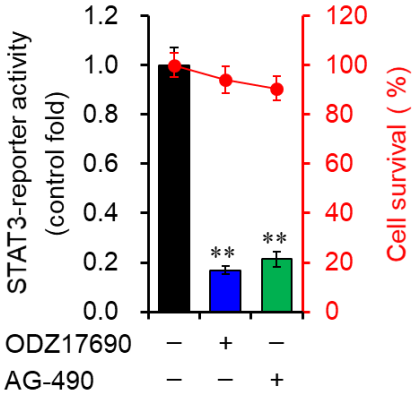

Figure 2. Identification of ODZ17690 as a hit compound by targeting the SH2 domain of STAT3.

(A) Docked model of ODZ17690 is shown in stick and the surrounding residues of the SH2 domain of STAT3 are shown by a line model. Hydrogen bonds are shown for Ser611 and Glu638. A salt bridge and attractive charge type interactions are observed between the Lys591 and Arg609 and nitro group O of ODZ17690. (B) 2D-interaction image is shown and various interaction types are color coded. (C) MDA-MB-231/STAT3-Luc cells were incubated for 24 h with vehicle (0.1% DMSO) alone, ODZ17690 (150 μM), or AG-490 (150 μM), and STAT3-reporter activity and cell viability were determined [5].

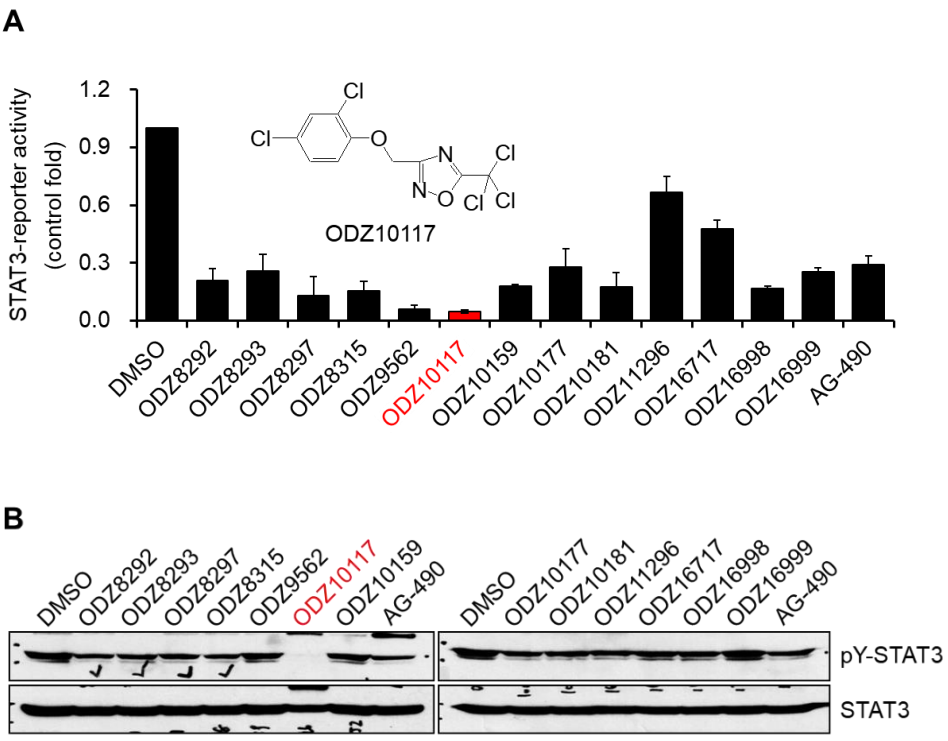

Figure 3. Identification of ODZ10117 as a STAT3 inhibitor from the optimization of ODZ17690.

(A) MDA-MB-231/STAT3-Luc cells were incubated for 24 h with vehicle (0.1% DMSO) alone or each ODZ17690 derivative (40 μM), and STAT3-reporter activity was determined. Results are represented as mean ± SEM of three independent experiments (n = 3). Chemical structure of ODZ10117 is represented. (D) MDA-MB-231 cells were incubated for 24 h with either vehicle (0.1% DMSO) or each compound (40 μM) and immunoblot analysis was performed. Results shown represent only 13 compounds of the 144 derivatives of ODZ17690. AG-490 was used as a positive control [5].

A

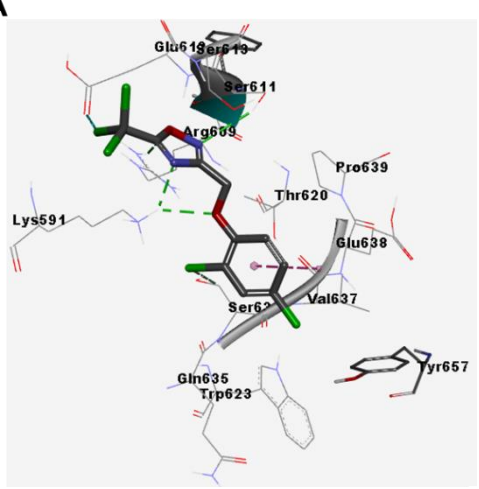

B

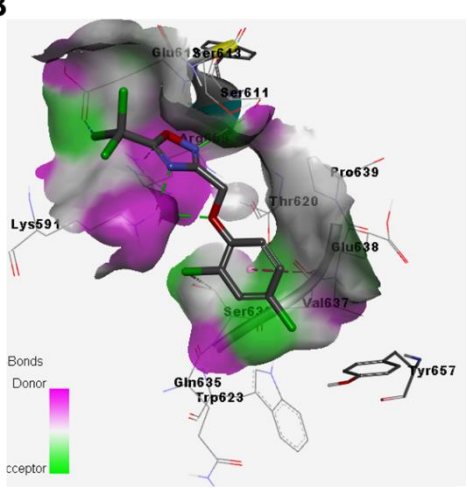

C

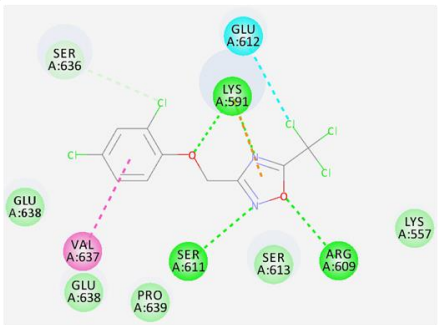

van der Waals
Halogen
Conventional Hydrogen Bond
Amide-Pi Stacked
Carbon Hydrogen Bond
Alkyl, Pi-Alkyl
Attractive Charge, Pi-Cation, Salt Bridge

D

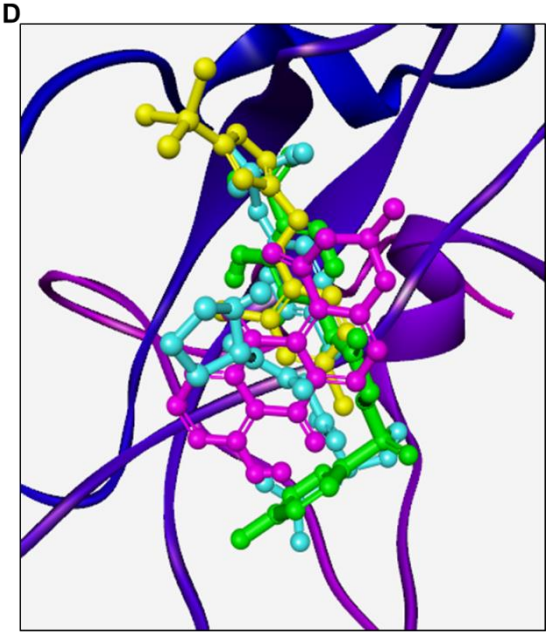

van der Waals
Conventional Hydrogen Bond
Pi-Donor Hydrogen Bond
Attractive Charge, Pi-Cation, Salt Bridge
Halogen
Amide-Pi Stacked
Alkyl, Pi-Alkyl

E

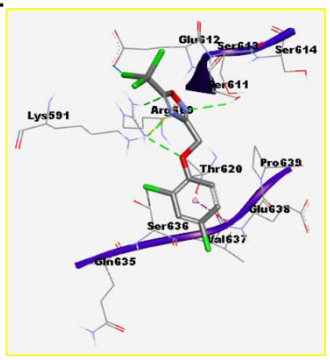

F

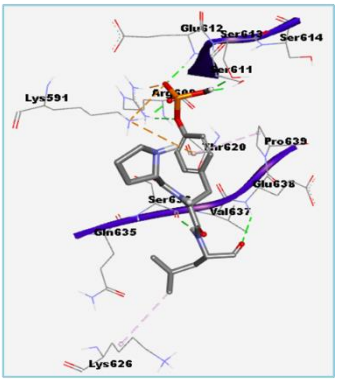

G

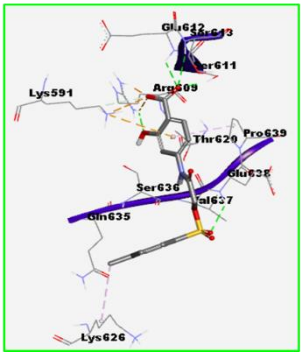

H

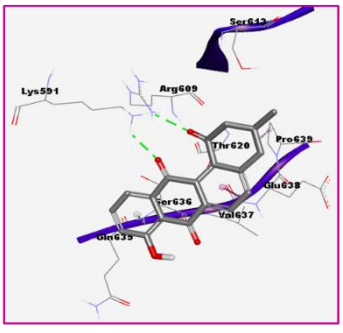

Figure 4. Molecular docking of ODZ10117 against the SH2 domain of STAT3.

(A) Docked model of ODZ10117 is shown in stick and the surrounding residues of the SH2 domain of STAT3 are shown by a line model. Hydrogen bonds are shown for Lys591, Arg609, and Ser611. Halogen bond between Cl and Glu612 is shown by a cyan dash. (B) Transparent hydrogen bond acceptor/donor surface is shown for surrounding residues. (C) 2D-interaction plot is shown and color-coded by various interaction types. (D) Superimposed docked models of ODZ10117 (yellow), Pro-pTyr-Leu (cyan), S3I-201 (green), and STA-21 (magenta) over STAT3. (E-H) Docked models of ODZ10117 (E), Pro-pTyr-Leu (F), S3I-201 (G), and STA-21 (H) surrounding 4Å residues of STAT3. Color codes for the different types of interactions are shown at the bottom of D [5].

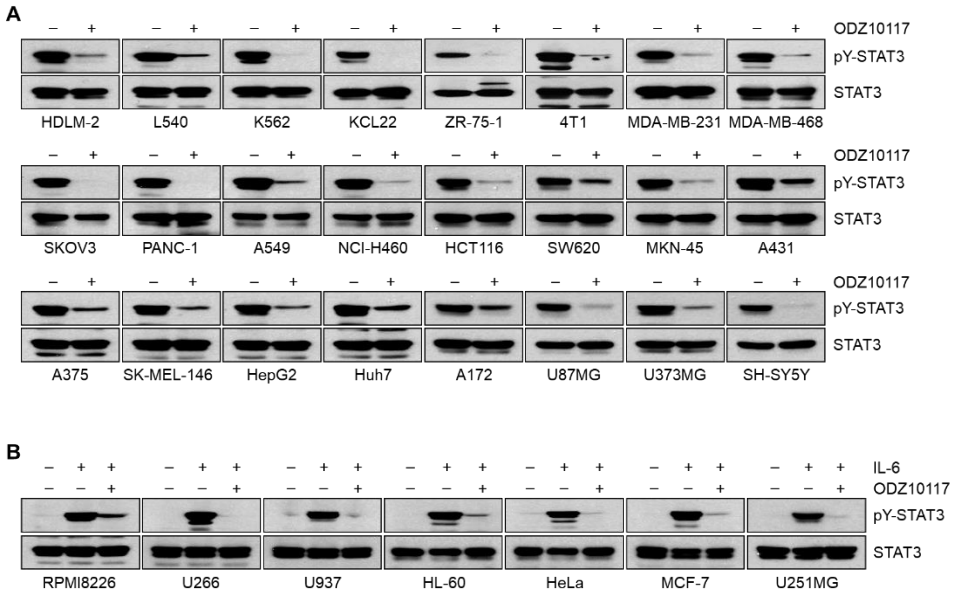

Figure 5. ODZ10117 inhibits tyrosine phosphorylation of STAT3 in various human cancer cell lines.

(A, B) Various types of human cancer cell lines with STAT3 constitutively activated (A) or activated by IL-6-stimulation (20 ng/mL) for 10 min (B) were incubated for 24 h with either vehicle (0.1% DMSO) alone or ODZ10117 (40 μM) and immunoblotting was performed [5].

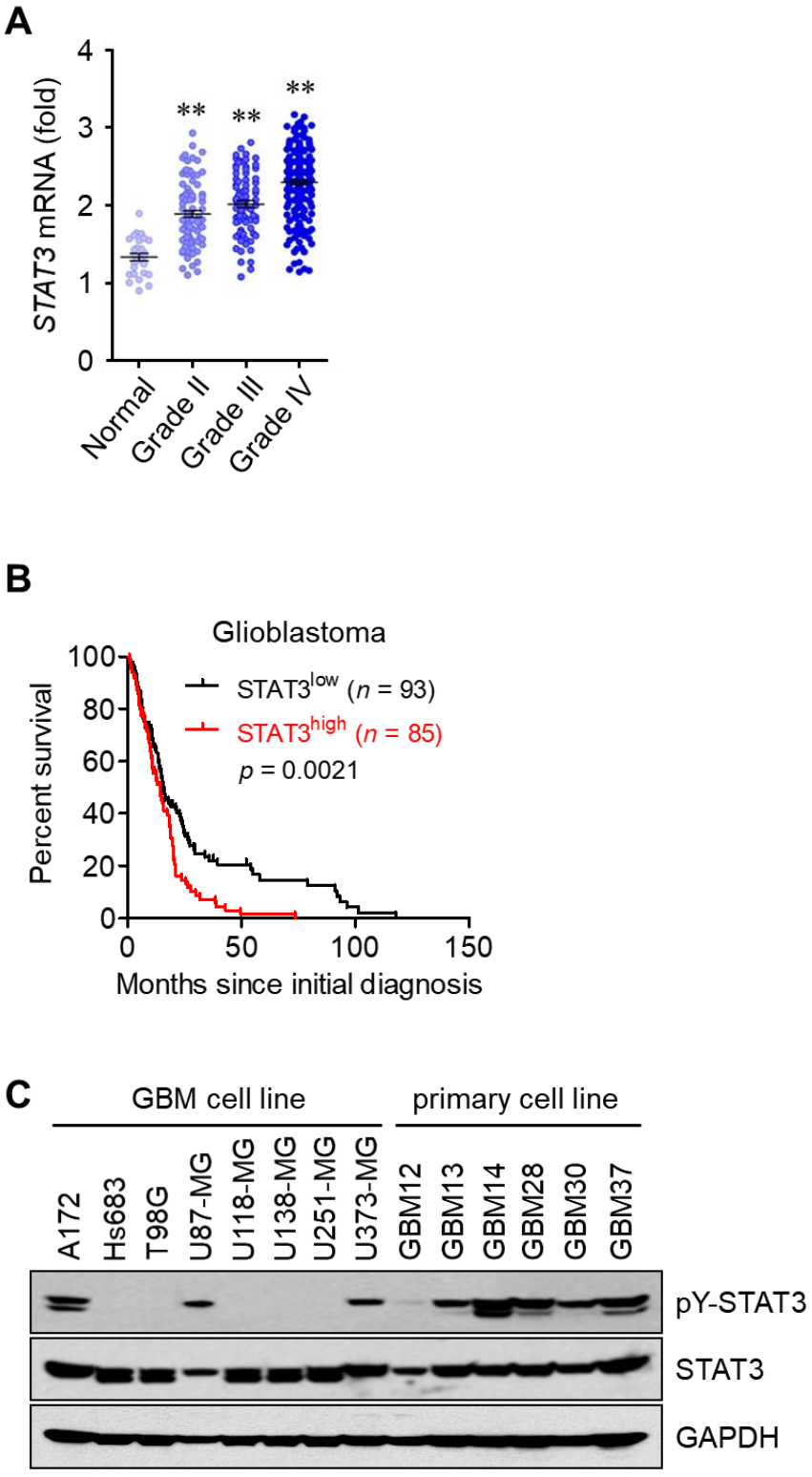
A
STAT3 mRNA (fold)
4
3
2
1
0
**
**
**
Normal
Grade II
Grade III
Grade IV
B
Glioblastoma
Percent survival
100
80
60
40
20
0
STAT3low (n = 93)
STAT3high (n = 85)
p = 0.0021
0
50
100
150
Months since initial diagnosis
C
GBM cell line
primary cell line
A172
Hs683
T98G
U87-MG
U118-MG
U138-MG
U251-MG
U373-MG
GBM12
GBM13
GBM14
GBM28
GBM30
GBM37
pY-STAT3
STAT3
GAPDH

Figure 6. STAT3 hyperactivation is associated with tumor malignancy and survival in glioblastoma patients.

(A) The mRNA level of STAT3 in patients with gliomas of various grades. Results were analyzed from TCGA database. * $p < 0.05$ and ** $p < 0.005$. (B) Kaplan–Meier survival curves for patients with glioblastomas. Data from the TCGA database. (C) Western blot results of glioblastoma and primary glioblastoma cell lines established from the patients [74].

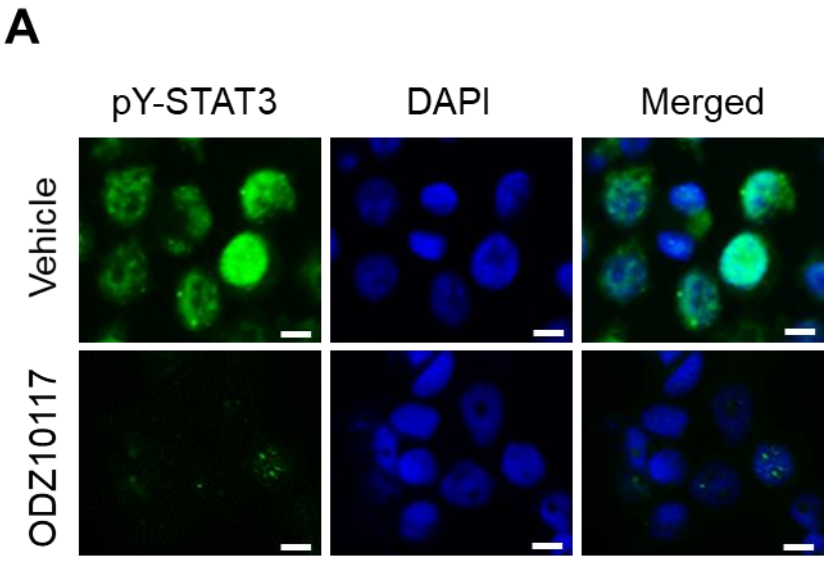
A
pY-STAT3
DAPI
Merged
Vehicle
ODZ10117

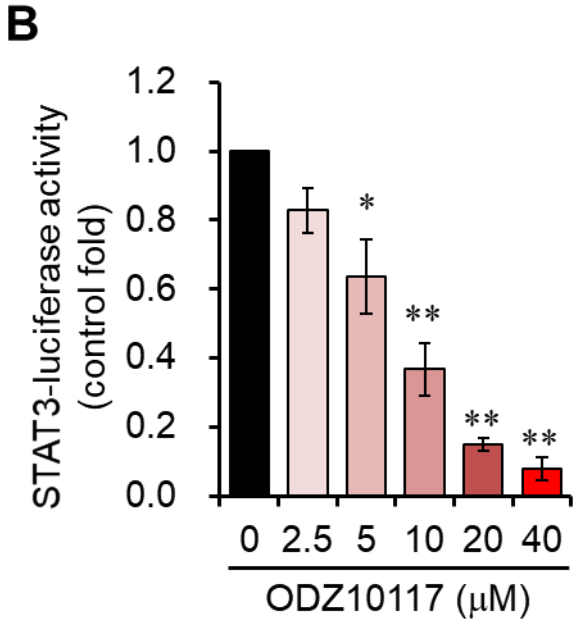
B
STAT3-luciferase activity
(control fold)
1.2
1.0
0.8
0.6
0.4
0.2
0.0
*
**
**
**
0
2.5
5
10
20
40
ODZ10117 (μM)

Figure 7. ODZ10117 inhibits STAT3 signaling *in vitro.*

(A) Immunofluorescence (IF) staining was performed using an anti-pY^{705}-STAT3 antibody (green) in U87MG cells incubated for 24 hours with vehicle (0.1% DMSO) alone or ODZ10117 (40 μM). Nuclei were stained with DAPI (blue). Arrowheads indicate nuclear phosphotyrosine STAT3. (B) STAT3 reporter assay of U87MG cells treated for 24 hours with ODZ10117. Cells were transfected with the p21×STAT3-firefly luciferase reporter gene and the pRL-TK *Renilla* luciferase reporter gene. Data are represented as mean ± SEM of three independent experiments. * $p < 0.05$ and ** $p < 0.005$ compared to the vehicle-treated group [5].

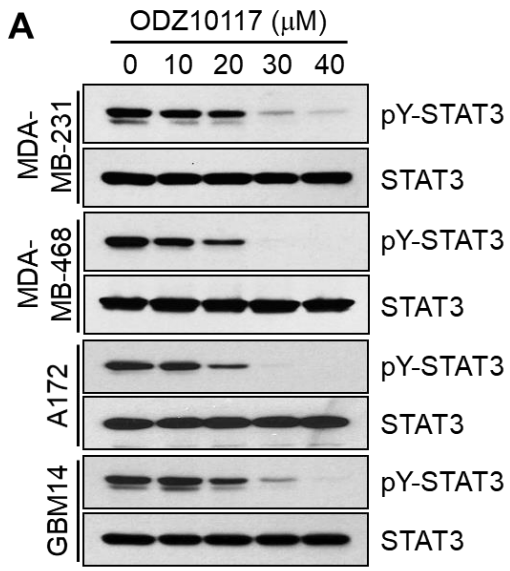
A
ODZ10117 (μM)
0 10 20 30 40
MDA-MB-231
pY-STAT3
STAT3
MDA-MB-468
pY-STAT3
STAT3
A172
pY-STAT3
STAT3
GBM14
pY-STAT3
STAT3

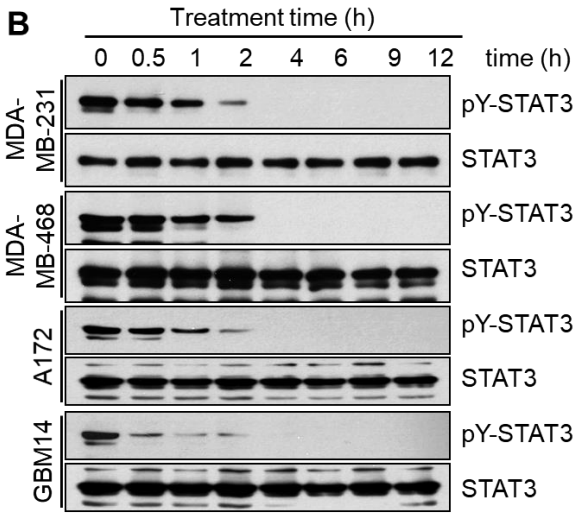
B
Treatment time (h)
0 0.5 1 2 4 6 9 12 time (h)
MDA-MB-231
pY-STAT3
STAT3
MDA-MB-468
pY-STAT3
STAT3
A172
pY-STAT3
STAT3
GBM14
pY-STAT3
STAT3

Figure 8. ODZ10117 inhibits STAT3 activation in a concentration-and time-dependent manner.

(A) Cells were treated for 9 h in a concentration-dependent manner. (B) Cells were treated with ODZ10117 (40 μM) in a time-dependent manner [5, 74].

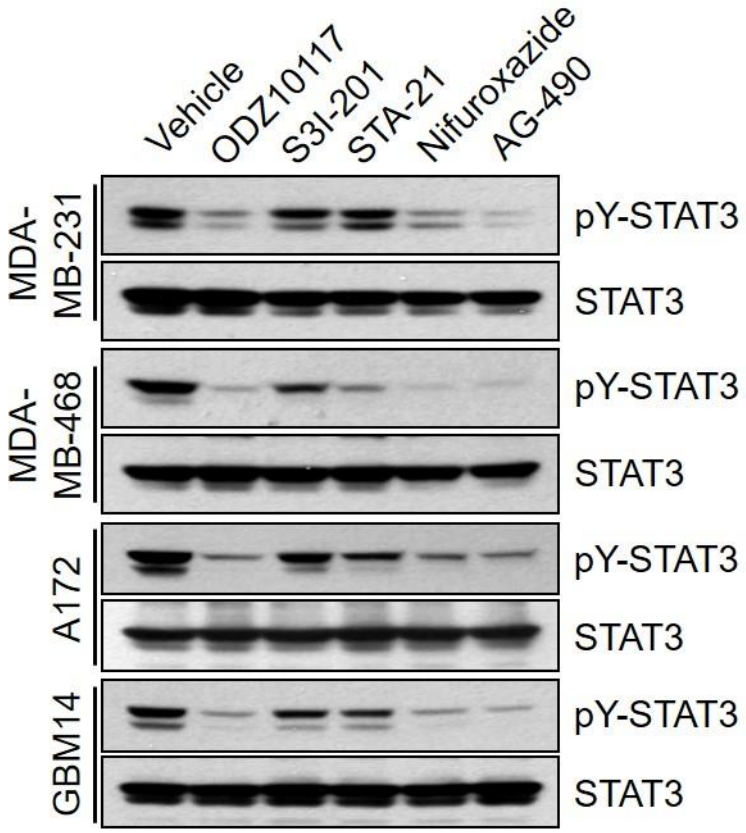

Figure 9. ODZ10117 has a greater inhibition on STAT3 activation than the known inhibitors.

Comparison on the effects of ODZ10117 (40 μM) and the known STAT3 inhibitors S3I-201 (100 μM), STA-21 (100 μM), nifuroxazide (NIF, 100 μM), and AG-490 (150 μM) on tyrosine phosphorylation of STAT3. Cells were incubated for 12 h with each compound and then performed immunoblot analysis [5, 74].

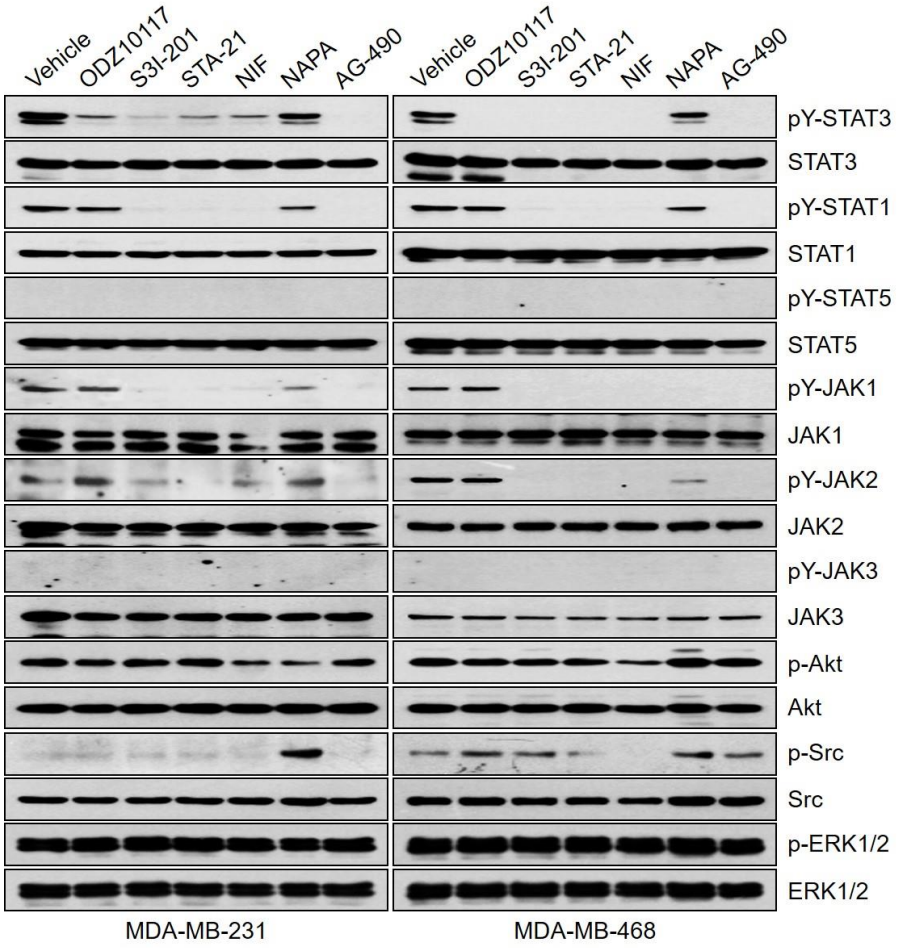

Figure 10. ODZ10117 does not affect STAT1 or upstream regulators of STAT3 in breast cancer cells.

Cells were incubated for 16 h with vehicle (0.1% DMSO) alone, ODZ10117 (ODZ, 40 μM) or the known STAT3 inhibitors S3I-201 (100 μM), STA-21 (100 μM), nifuroxazide (NIF, 100 μM), napabucasin (NAPA, 4 μM), or AG-490 (150 μM), and then performed immunoblot analysis [5].

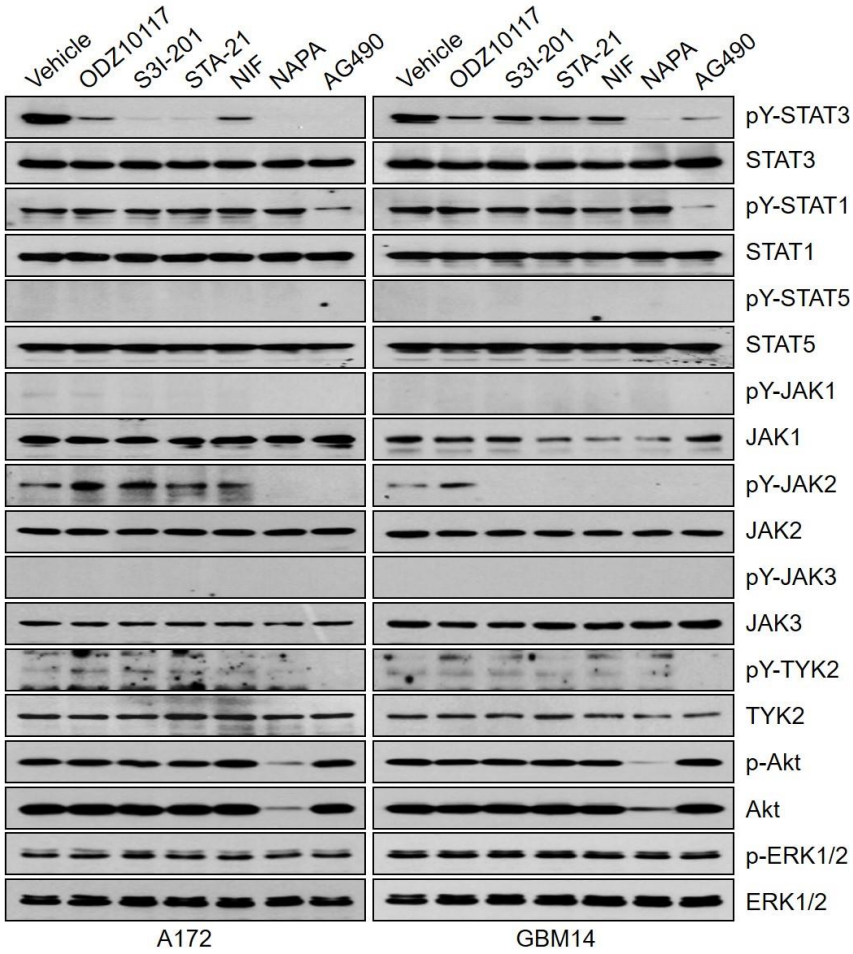

Figure 11. ODZ10117 does not affect STAT1 or upstream regulators of STAT3 in glioblastoma cells.

Western blotting was performed from the cells incubated for 24 hours with ODZ10117 (40 μM) or the known STAT3 inhibitor S3I-201 (100 μM), STA-21 (100 μM), nifuroxazide (100 μM), napabucasin (NAPA, 4 μM), or AG-490 (150 μM).

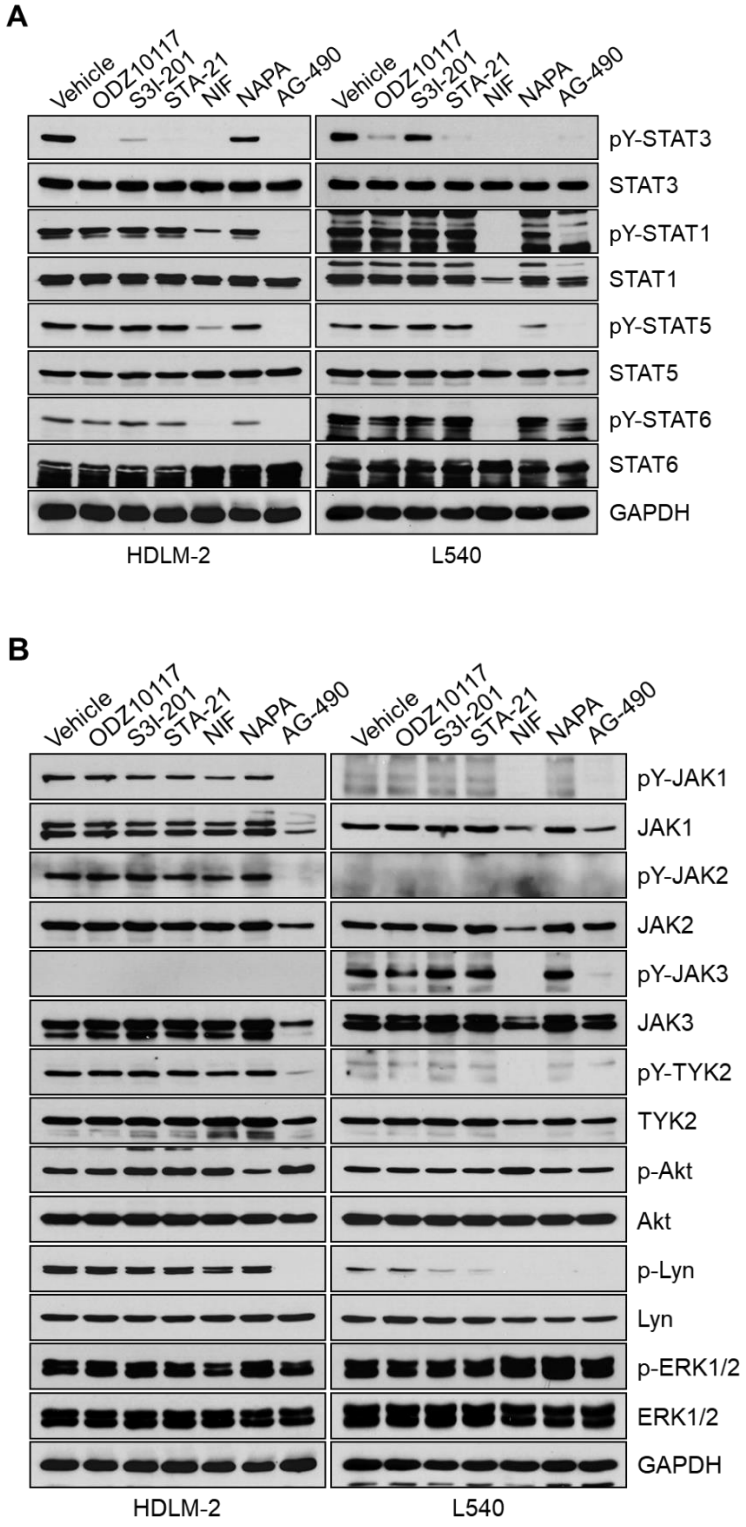
A
Vehicle
ODZ10117
S3I-201
STA-21
NIF
NAPA
AG-490
pY-STAT3
STAT3
pY-STAT1
STAT1
pY-STAT5
STAT5
pY-STAT6
STAT6
GAPDH
HDLM-2
L540
B
pY-JAK1
JAK1
pY-JAK2
JAK2
pY-JAK3
JAK3
pY-TYK2
TYK2
p-Akt
Akt
p-Lyn
Lyn
p-ERK1/2
ERK1/2
GAPDH
HDLM-2
L540

Figure 12. ODZ10117 does not affect other STAT family members or upstream regulators of STAT3 in Hodgkin's lymphoma cells.
(A, B) Western blotting was performed from HLDM-2 and L540 cells incubated for 24 hours with ODZ10117 (40 μM) or the known STAT3 inhibitor S3I-201 (100 μM), STA-21 (100 μM), nifuroxazide (100 μM), napabucasin (4 μM), or AG-490 (150 μM) [5].

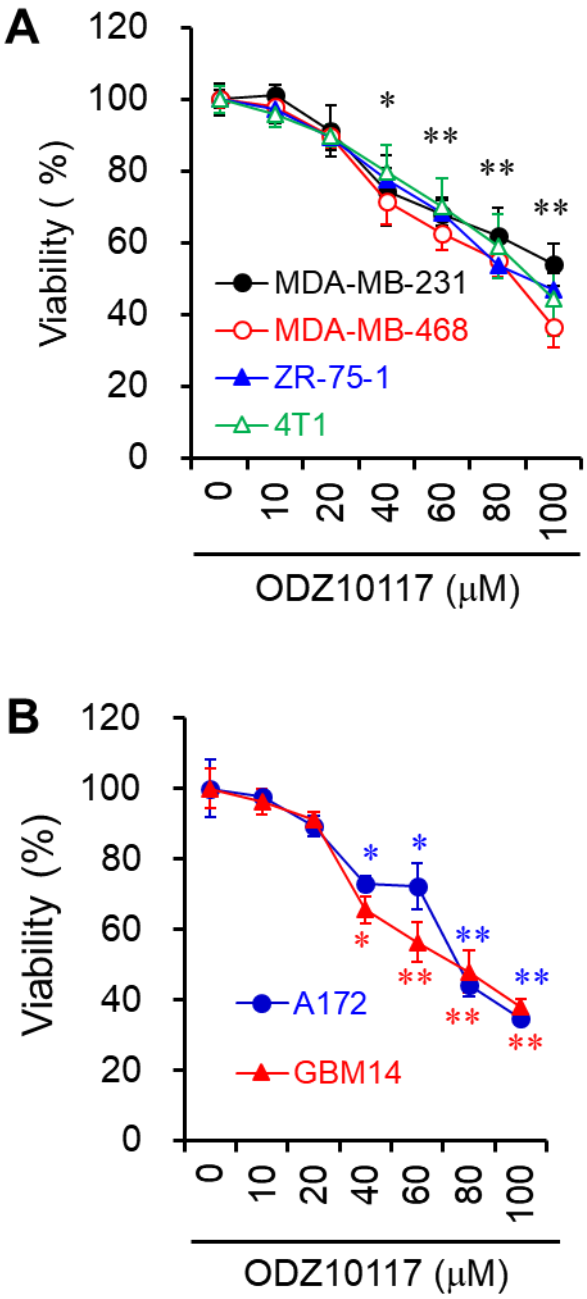

Figure 13. ODZ10117 decreases cell viability.

(A, B) Cells were incubated for 24 h with various concentrations of ODZ10117 and cell viability was determined [5, 74].

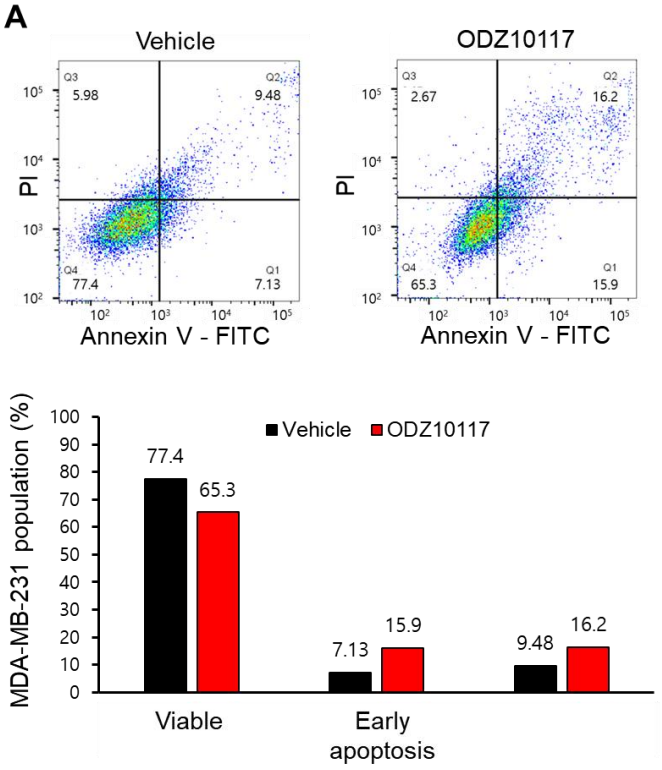
A
Vehicle
ODZ10117
PI
Annexin V - FITC
Q3
Q2
Q4
Q1
5.98
9.48
77.4
7.13
2.67
16.2
65.3
15.9
MDA-MB-231 population (%)
Vehicle
ODZ10117
77.4
65.3
7.13
15.9
9.48
16.2
Viable
Early apoptosis

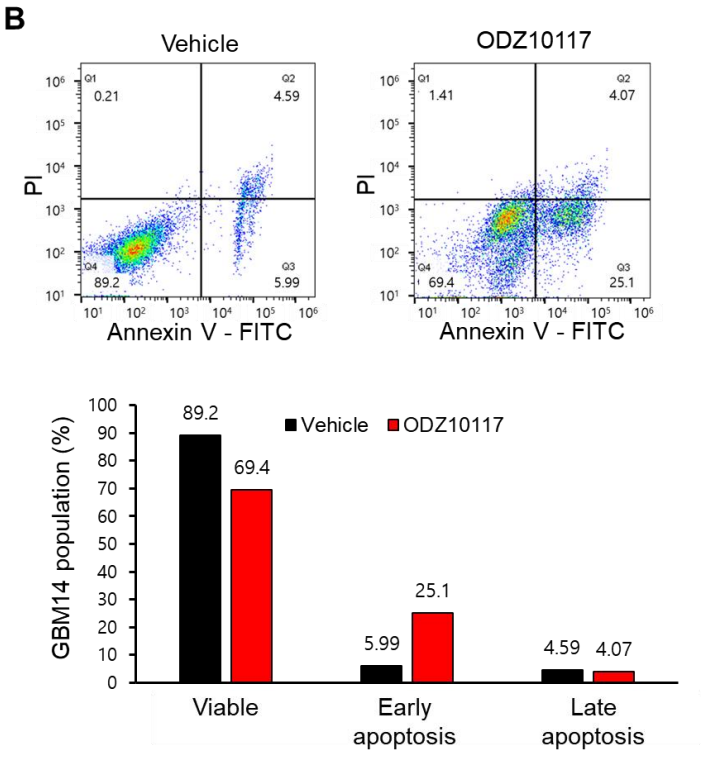
B
Vehicle
ODZ10117
PI
Annexin V - FITC
Q1
Q2
Q4
Q3
0.21
4.59
89.2
5.99
1.41
4.07
69.4
25.1
GBM14 population (%)
Vehicle
ODZ10117
89.2
69.4
5.99
25.1
4.59
4.07
Viable
Early apoptosis
Late apoptosis

Figure 14. ODZ10117 decreases the viability of breast cancer and glioblastoma cells by inducing apoptosis.

(A, B) MDA-MB-231 cells or GBM14 cells were incubated for 24 h with vehicle (0.1% DMSO) alone or ODZ10117 (40 μM) and then performed FACS analysis.

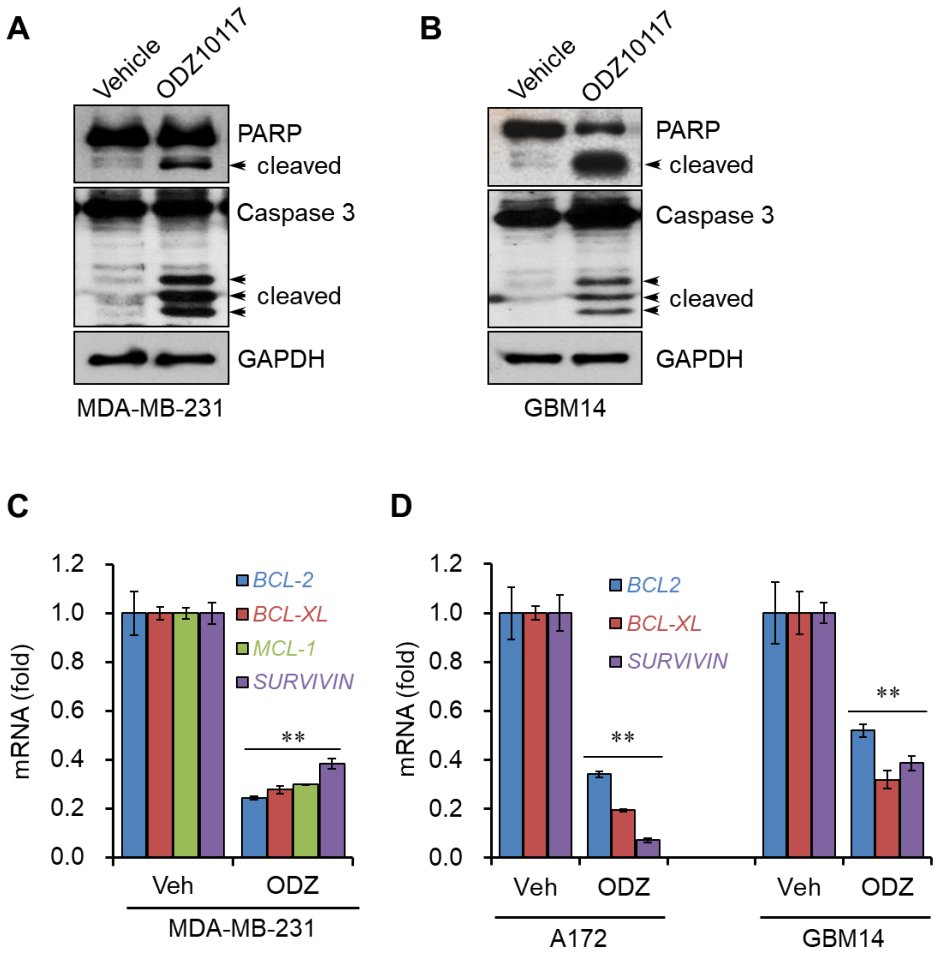

Figure 15. ODZ10117 induces apoptotic cell death in breast cancer and glioblastoma cells.

(A–D) MDA–MB–231 cells, A172 or GBM14 cells were incubated for 24 h with vehicle (0.1% DMSO) alone or ODZ10117 (40 μM) and and subjected to Western blot (A, B), and qPCR (C, D) analyses. *GAPDH* served as the loading control and data represent the mean ± SEM of three independent experiments. ** p <0.005 [5, 74].

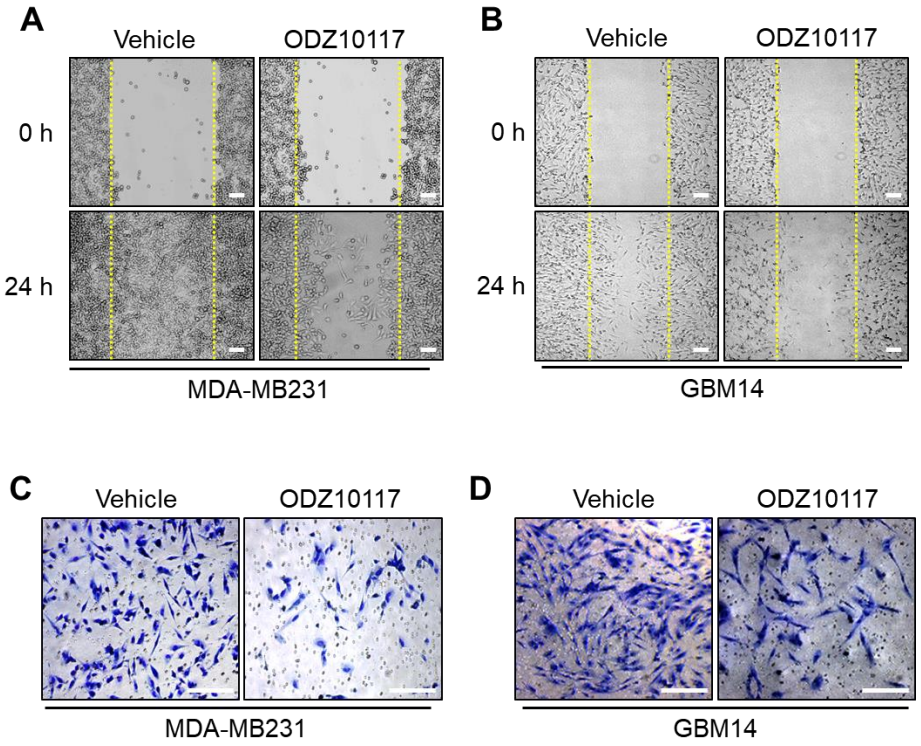

Figure 16. ODZ10117 decreases the migration and invasion in breast cancer and glioblastoma cells.

(A–D) Wound healing (A, B) and Matrigel invasion (C, D) assays of cells from MDA–MB231 or GBM14 incubated for 24 h with vehicle (0.1% DMSO) alone or ODZ10117 (40 μM). The images were visualized by phase–contrast microscopy (magnification = 200×) [5, 74].

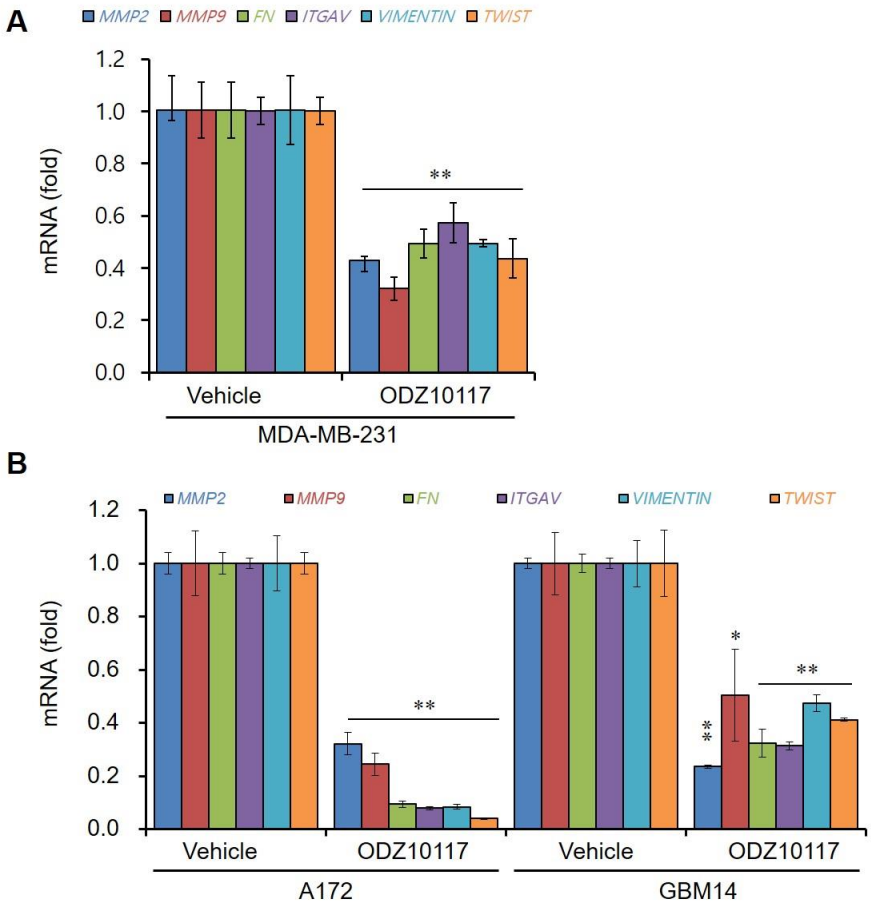

Figure 17. ODZ10117 decreases the expression of STAT3 target genes associated with migration and invasion.

(A, B) qPCR analyses were performed in breast cancer or glioblastoma cells incubated for 24 h with vehicle (0.1% DMSO) alone or ODZ10117 (40 μM). *GAPDH* served as the loading control and data represent the mean ± SEM of three independent experiments. * $p < 0.05$ and ** $p < 0.005$ [5, 74].

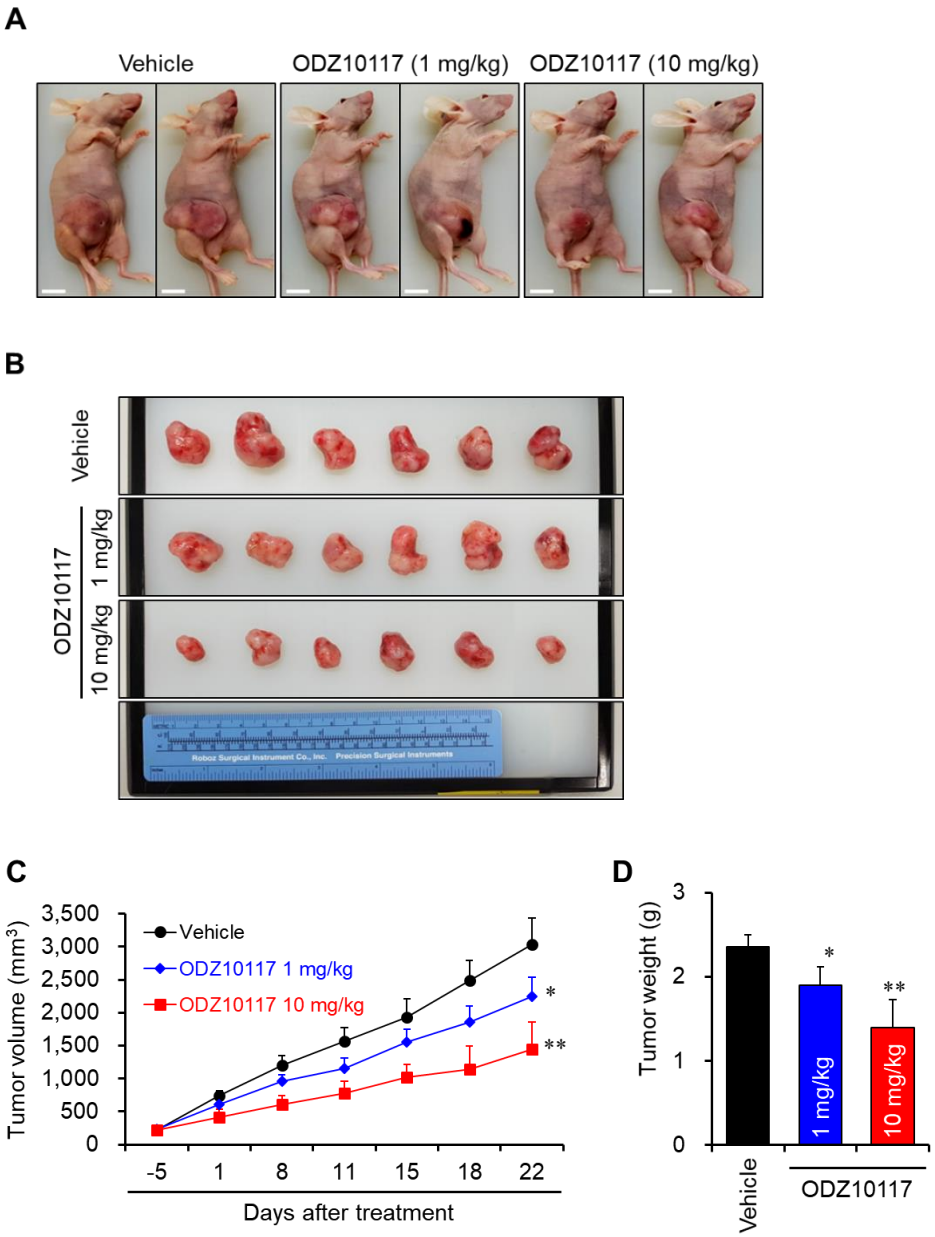
A
Vehicle
ODZ10117 (1 mg/kg)
ODZ10117 (10 mg/kg)
B
Vehicle
ODZ10117
1 mg/kg
10 mg/kg
C
Tumor volume (mm3)
3,500
3,000
2,500
2,000
1,500
1,000
500
0
Vehicle
ODZ10117 1 mg/kg
ODZ10117 10 mg/kg
*
**
-5
1
8
11
15
18
22
Days after treatment
D
Tumor weight (g)
3
2
1
0
*
**
1 mg/kg
10 mg/kg
Vehicle
ODZ10117

Figure 18. ODZ10117 suppressed tumor growth in breast cancer xenograft models.

(A–D) Orthotopic xenograft model was generated by injection of MDA-MB-231 cells into the right fourth mammary fat pad of female BALB/c mice. The tumor growth (A), tumor size (B), tumor growth curve (C), and tumor weight (D) were represented [5].

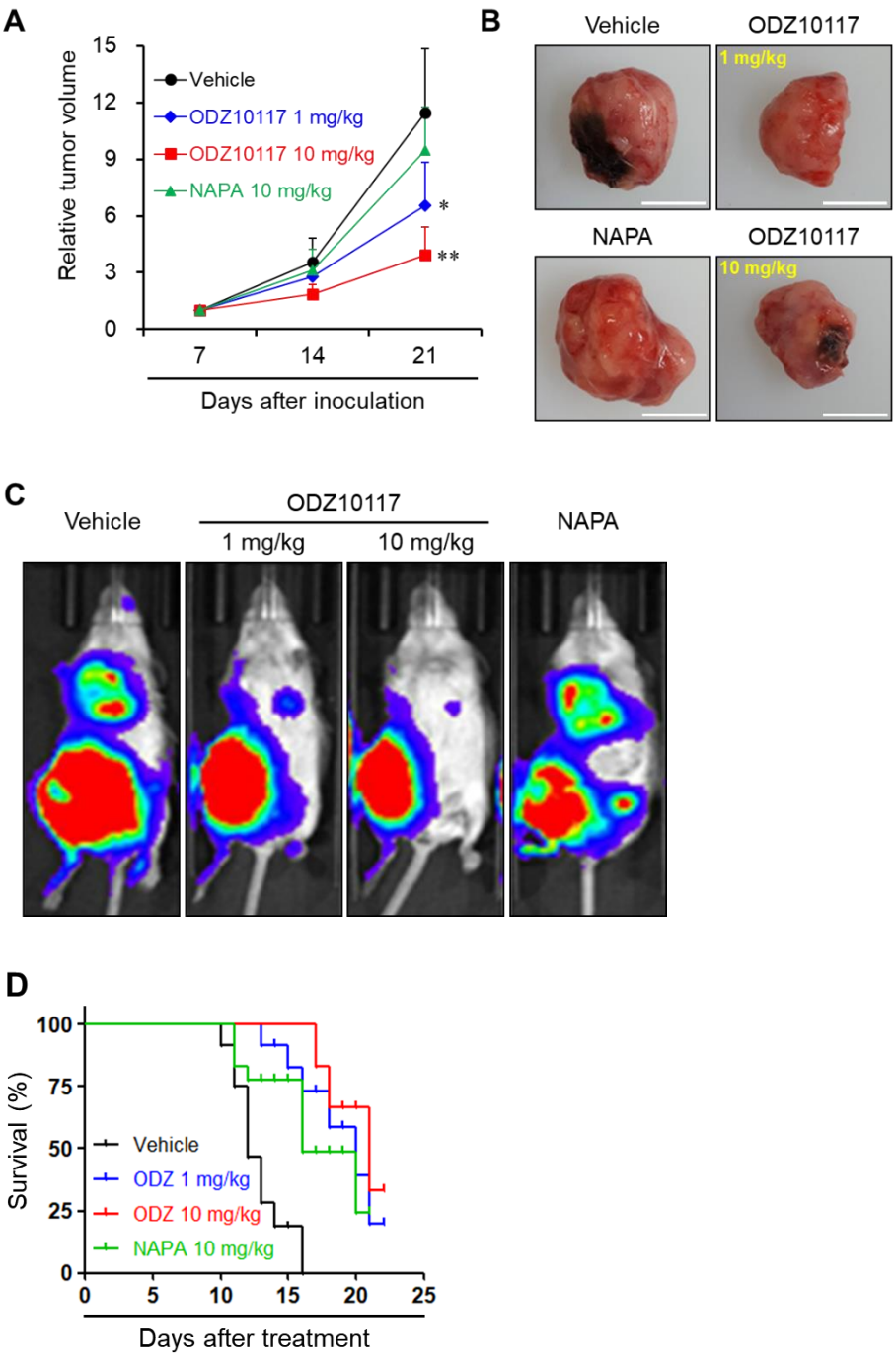
A
Relative tumor volume
15
12
9
6
3
0
Vehicle
ODZ10117 1 mg/kg
ODZ10117 10 mg/kg
NAPA 10 mg/kg
*
**
7
14
21
Days after inoculation
B
Vehicle
ODZ10117
1 mg/kg
NAPA
ODZ10117
10 mg/kg
C
Vehicle
ODZ10117
1 mg/kg
10 mg/kg
NAPA
D
Survival (%)
100
75
50
25
0
Vehicle
ODZ 1 mg/kg
ODZ 10 mg/kg
NAPA 10 mg/kg
0
5
10
15
20
25
Days after treatment

Figure 19. ODZ10117 inhibits tumor growth and increases survival in metastatic breast cancer xenograft model.

(A–D) Syngeneic breast metastasis xenograft model was generated by injection of 4T1-Luc cells into the right fourth mammary fat pad of female BALB/c mice. Primary tumor growth is shown (A, B). Representative bioluminescence images of whole body (C). Kaplan-Meier survival graph of tumor-bearing mice (D). * $p < 0.05$ and ** $p < 0.005$ compared to the vehicle-treated group [5].

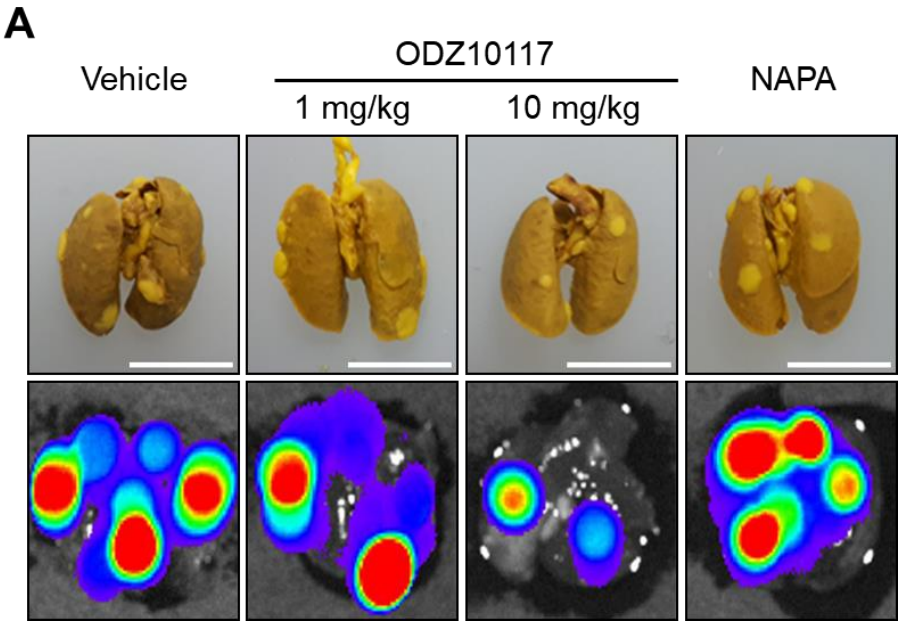
A
Vehicle
ODZ10117
1 mg/kg
10 mg/kg
NAPA

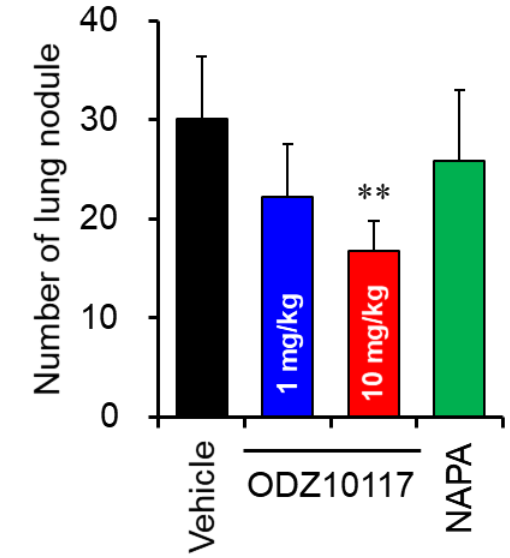
B
Number of lung nodule
40
30
20
10
0
**
1 mg/kg
10 mg/kg
Vehicle
ODZ10117
NAPA

Figure 20. ODZ10117 inhibits lung metastasis in breast cancer xenograft model.

(A–B) Syngeneic breast metastasis xenograft model was generated by injection of 4T1-Luc cells into the right fourth mammary fat pad of female BALB/c mice. Lung metastatic tumor nodules were observed on the surface (upper) and bioluminescence images (bottom) of the lung (A) and lung nodules were counted (B). * $p < 0.05$ and ** $p < 0.005$ compared to the vehicle-treated group [5].

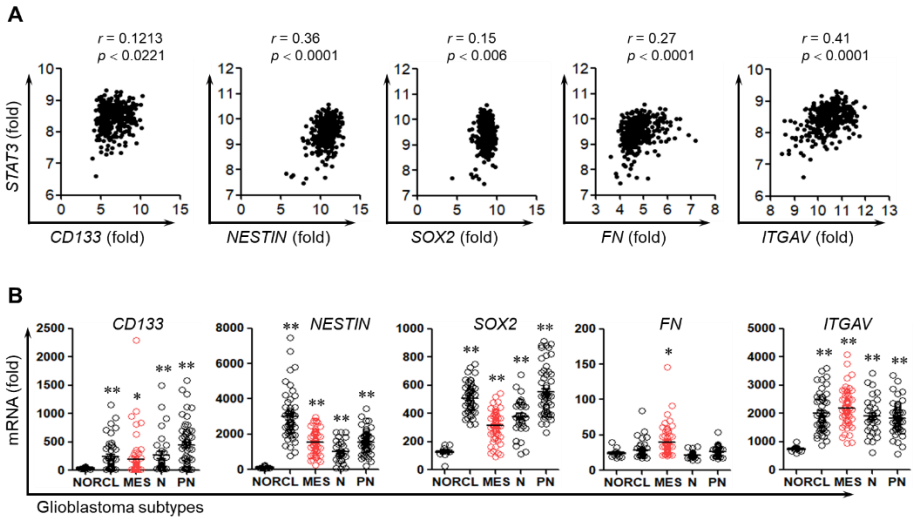

Figure 21. Positive correlation between STAT3 and stem cell phenotypes and EMT markers in glioblastoma patients.

(A) Positive correlations of the mRNA levels between STAT3 and *CD133, NESTIN, SOX2, FN*, and *ITGAV*. (B) The mRNA levels of *CD133, NESTIN, SOX2, FN*, and *ITGAV* are elevated in different subtypes of glioblastoma patients. * $p < 0.05$ and ** $p < 0.005$. Data from the TCGA database [74].

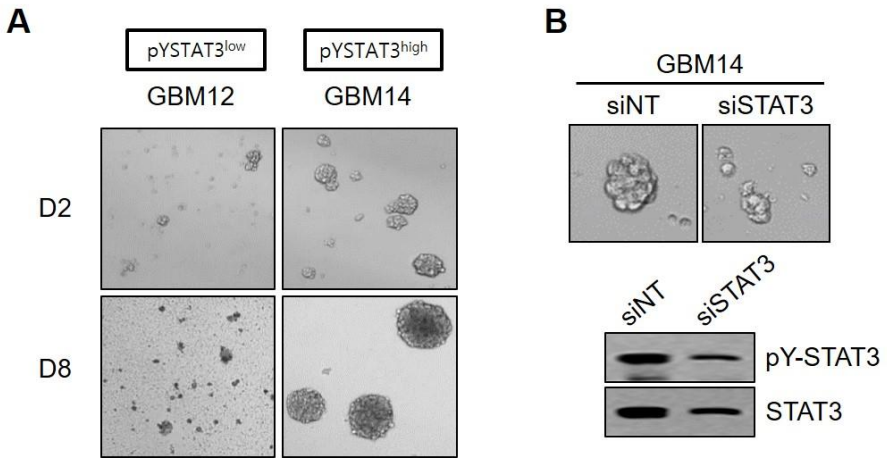

Figure 22. STAT3 expression regulates tumorspere-forming capacity of glioblastoma cells.

(A, B) Sphere-forming assay was performed in GBM12 and GBM14 cells following incubation for 2 or 8 days (A), or in GBM14 cells transfected with the control or STAT3 siRNA following incubation for 8 days (B) under stem cell culture conditions [74].

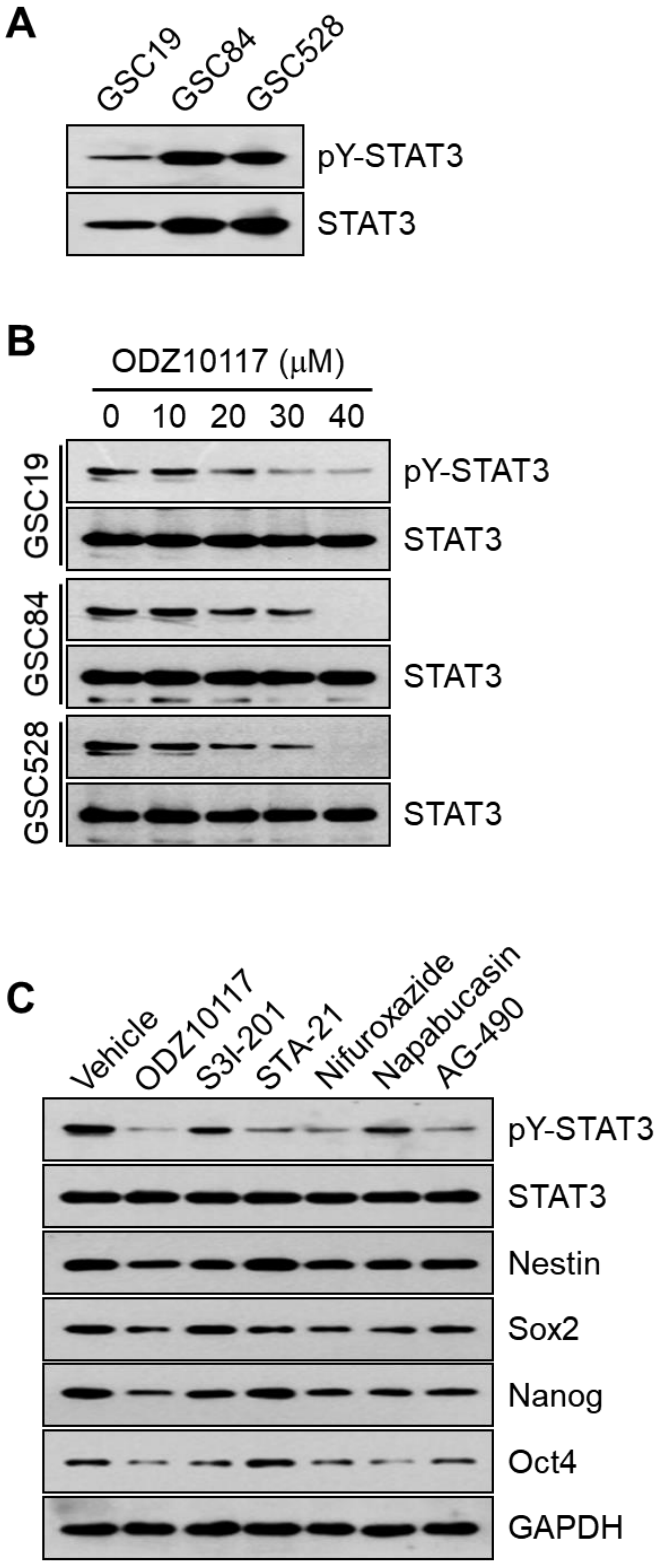
A
GSC19
GSC84
GSC528
pY-STAT3
STAT3
B
ODZ10117 (μM)
0 10 20 30 40
GSC19
pY-STAT3
STAT3
GSC84
STAT3
GSC528
STAT3
C
Vehicle
ODZ10117
S3I-201
STA-21
Nifuroxazide
Napabucasin
AG-490
pY-STAT3
STAT3
Nestin
Sox2
Nanog
Oct4
GAPDH

Figure 23. ODZ10117 suppresses STAT3 activation and cancer stem cell markers in GSCs.

(A) The levels of pY-STAT3 and STAT3 in GSCs were determined by Western blot analysis. (B, C) Western blot analysis was performed for STAT3 activation and/or stem cell markers in GSCs incubated for 24 h with ODZ10117 (C) and in GSC528 cells incubated for 24 h with ODZ10117 and the known STAT3 inhibitors (D). GAPDH served as the loading control. ODZ10117 (40 μM), S3I-201 (100 μM), STA-21 (100 μM), nifuroxazide (100 μM), napabucasin (4 μM), and AG-490 (150 μM)[74].

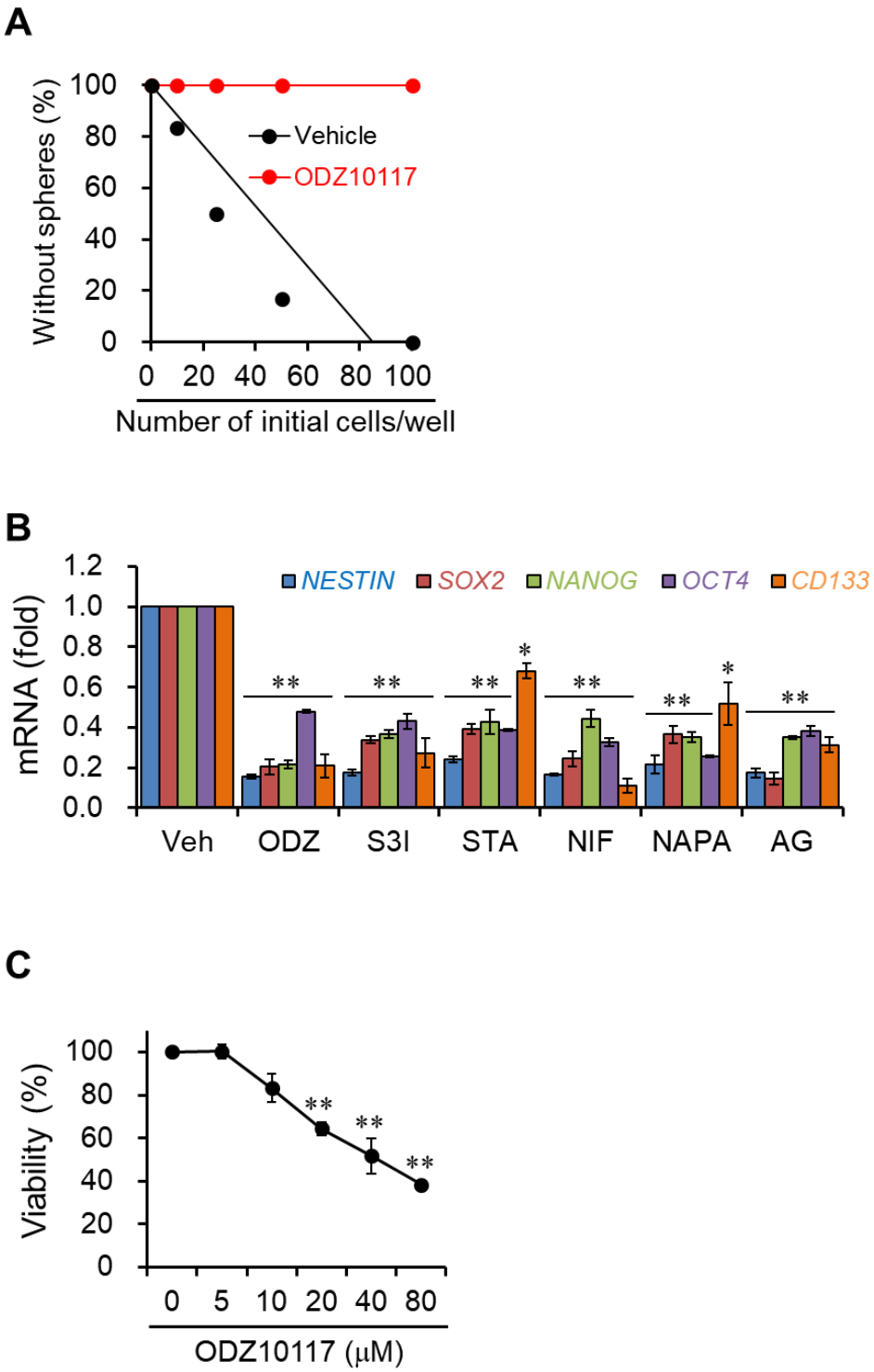
A
Without spheres (%)
100
80
60
40
20
0
Vehicle
ODZ10117
0 20 40 60 80 100
Number of initial cells/well
B
mRNA (fold)
1.2
1.0
0.8
0.6
0.4
0.2
0.0
NESTIN
SOX2
NANOG
OCT4
CD133
**
*
Veh
ODZ
S3I
STA
NIF
NAPA
AG
C
Viability (%)
100
80
60
40
20
0
**
0 5 10 20 40 80
ODZ10117 (μM)

Figure 24. ODZ10117 suppresses stemness features in GSCs.

(A) *In vitro* limiting dilution (n = 12) assays were performed in GSC528 cells incubated for 5 days with vehicle (0.1% DMSO) alone or ODZ10117. ODZ10117 (40 μM), S3I-201 (100 μM), STA-21 (100 μM), nifuroxazide (100 μM), napabucasin (4 μM), and AG-490 (150 μM). (B) The mRNA levels of the stem cell markers were determined by qPCR analyses in GSC528 cells incubated for 24 h with vehicle (0.1% DMSO) alone, ODZ10117 and the known STAT3 inhibitors. ODZ10117 (ODZ, 40 μM), S3I-201 (S3I, 100 μM), STA-21 (STA, 100 μM), nifuroxazide (NIF, 100 μM), napabucasin (NAPA, 4 μM), and AG-490 (AG, 150 μM). (C) Viability was determined in GSC528 cells incubated for 24 h with various concentrations of ODZ10117. Data represent the mean ± SEM of three independent experiments. * $p < 0.05$ and ** $p < 0.005$ [74].

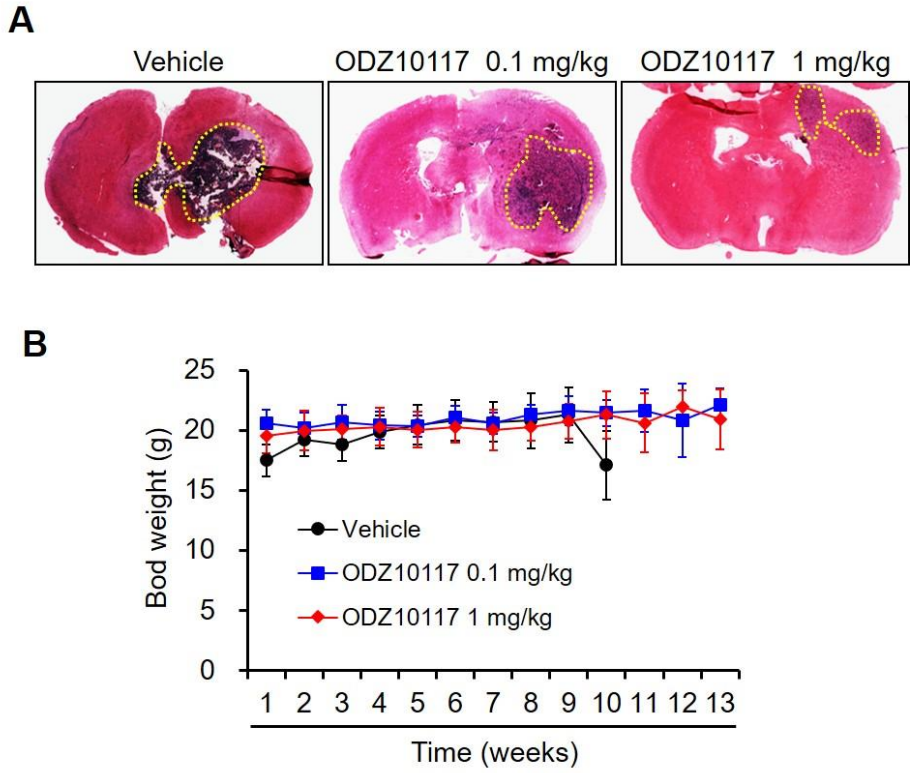

Figure 25. ODZ10117 reduces tumor growth in a glioblastoma xenograft model.

(A) glioblastoma orthotopic xenograft model was established by injecting GSC528 cells into the right striatum of 6-week-old BALB/c nu/nu nude mice (n = 6). H&E staining of mouse tumour tissues treated with vehicle alone or ODZ10117 (0.1 or 1 mg/kg). (B) Body weight of the tumour-bearing mice were determined [74].

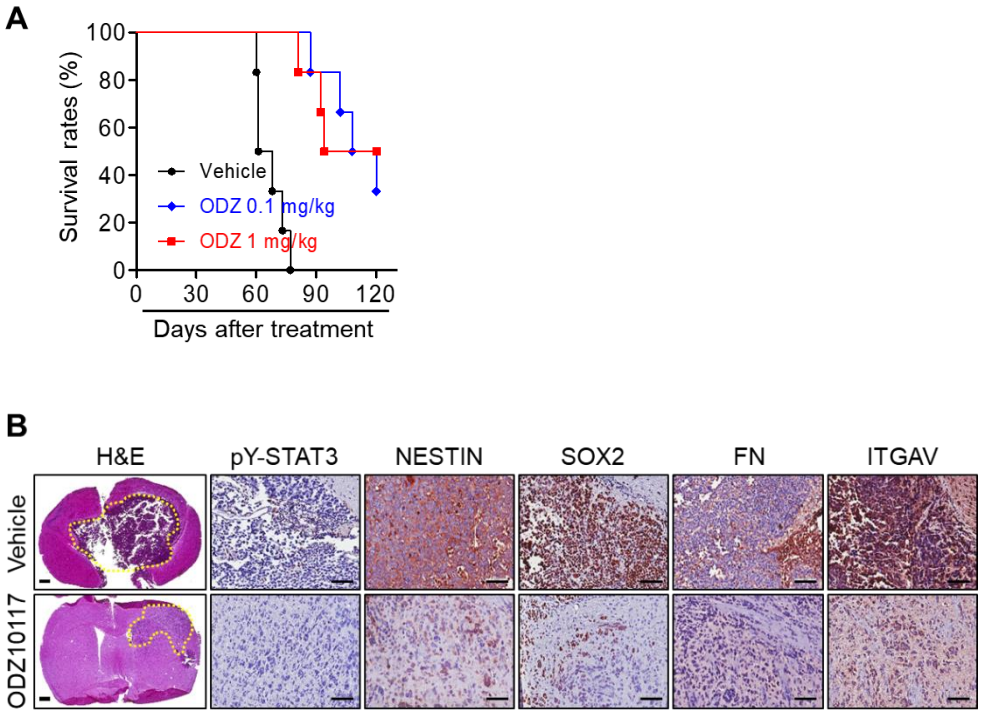

Figure 26. ODZ10117 reduces tumor growth in a glioblastoma xenograft model.

(A, B) Kaplan–Meier survival curves of tumor-bearing mice treated with vehicle alone or ODZ10117 (0.1 or 1 mg/kg, n = 6) (A). H&E and IHC staining of mouse tumor tissues were performed on day 77 after transplantation (B). Scale bar: 200 μm (IHC) or 500 μm (H&E) [74].

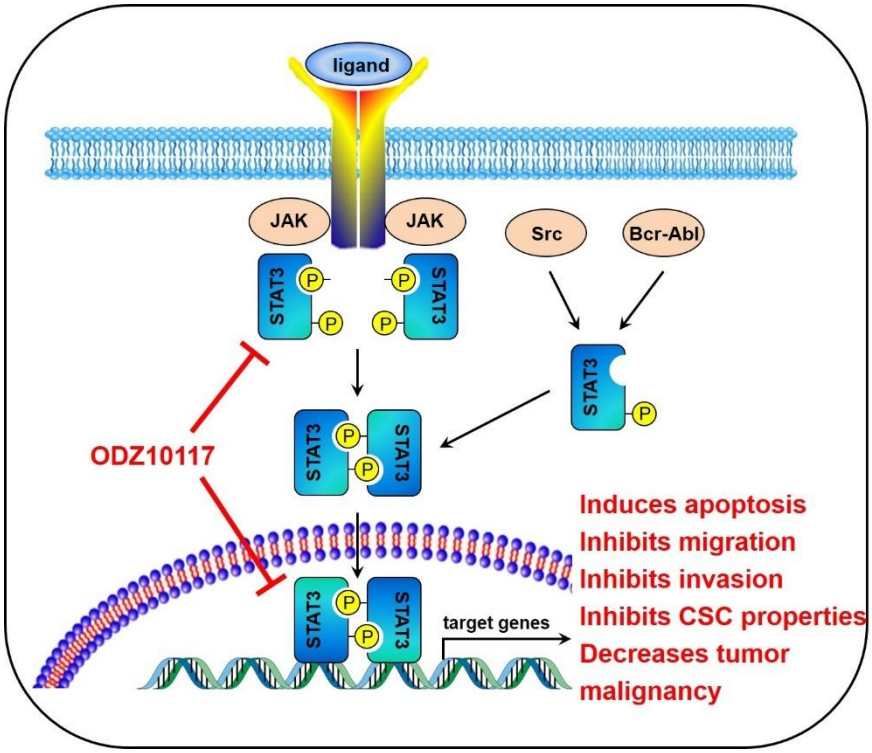

Figure 27. A schematic diagram illustrating the proposed action mechanism of ODZ10117.

ODZ10117 specifically targets the activation of STAT3, nuclear translocation, thereby inducing apoptotic cell death and reducing migration, invasion, cancer stem cell properties, and tumor growth, ultimately inhibiting cancer cell malignancy.

DISCUSSION

In the present study, I discovered ODZ10117 as a STAT3-specific inhibitor for STAT3-targeted cancer therapy and demonstrated its anticancer activities included the suppression of migration, invasion, viability, stem cell properties, and tumor growth, induction of apoptotic cell death, and extension of survival rate by targeting STAT3 in cancer cells and cancer xenografts (Figure 27).

Disrupted signaling pathways are generally associated with the development of many types of cancers[75], indicating that these signaling pathways can be promising therapeutic targets for cancer therapy and drug development. Among such pathways, aberrantly activated STAT3 signaling is considered an attractive therapeutic target for the treatment of many types of human diseases, including cancer [76, 77]. In fact, elevated activation of STAT3 is observed in many types of solid and hematological cancers, and has recently been suggested as an important target molecule in the pre-therapeutic assessment of cancer patients [57]. In particular, breast cancer remains the second most common type of cancer, a primary cause of death in women, and one of the most expensive malignancies to treat [78].

The survival rate of breast cancer patients depends on the diagnostic timing and characteristics of cancer cells. Survival is lower when the cancer is diagnosed at a later stage and the cancer cells show higher metastatic potential and CSC traits. These cases of cancer are responsible for the difficulty in treating and important factors in determining the prognosis of

breast cancer patients [49]. Specifically, higher level of tyrosine phosphorylated STAT3 was observed in TNBC subtype of breast cancer cells than those of other subtypes [79–81].

In addition, glioblastoma is a grade IV astrocytoma with very poor prognosis, according to the World Health Organization (WHO) [82]. It is the most aggressive and common primary adult brain tumor with a variety of characteristics featured by morphological and genetic heterogeneity [83]. Although there have been extensive advances in studies during the past decades, glioblastoma remains one of the most difficult types of cancers to treat because the exact causes are not clear and therapeutic strategies are limited. In addition, recurrence and resistance to conventional therapies occurs. Therefore, it is necessary to conduct extensive studies to identify the causes and develop novel therapeutic strategies for glioblastoma treatment.

According to recent studies, aberrantly activated STAT3 signaling is considered a paradigm for tumor initiation and malignancy, radio–chemoresistance, and recurrence due to observation in many types of cancers [58, 84, 85]. These correlations are mainly related to the functions of STAT3 in promoting the migration and invasion and maintaining stem cell properties of cancer cells, which indicates that STAT3 is an attractive molecular target for cancer therapy.

In fact, many compounds have been developed to inhibit STAT3 activity directly or indirectly [42, 81, 86]. Because the STAT family proteins and their upstream regulators can crosstalk with other signaling pathways associated with normal physiological functions, non–selective STAT3 inhibitors can

influence normal physiological functions. For this reason, the development of selective STAT3 inhibitors has many impediments. To date, only a few STAT3-specific inhibitors have been developed [19, 42, 69], but the inhibitors have not yet been studied in clinical trials. Therefore, the discovery of small-molecules specifically targeting STAT3 is an important issue for treating human diseases caused by STAT3 signaling.

In the present study, I performed two-track screening assays in combination with structure-based computational database screening and cell-based high-throughput screening to identify small-molecule inhibitors for STAT3-targeted cancer therapy. Finally, I discovered ODZ10117 as a novel STAT3-specific inhibitor and determined its pharmacological activities of ODZ10117 in both *in vitro* and *in vivo* models of breast cancer and glioblastoma. ODZ0117 is a led compound of STAT3 inhibitor and it is substituted by tri-chloride. The strength of substitution of chloride is that it is highly reactive molecule, but toxicity is caused, therefore, a stability evaluation is required. To be developed as an anti-cancer drug, further pharmacokinetics and toxicokinetics are needed.

Fortunately, ODZ10117 showed strong specificity for STAT3, regardless of other STAT family proteins and upstream regulators. Interestingly, I found that the known STAT3 inhibitors affected other STAT family proteins and upstream regulators, although they showed cell-line dependent effects, indicating that they are not STAT3-specific inhibitors. The STAT3-specificity and the STAT3 inhibitory effect of ODZ10117 were much stronger than that of the known STAT3

inhibitors such as S3I-201, STA-201, nifuroxazide, and napabucasin. So far, my findings are noteworthy that it has better efficacy of other commercial STAT3 inhibitors.

Although these results demonstrate the inhibitory effects of STAT3 in cancer cells, further detailed mechanism studies are needed for more clarification. Although ODZ10117 has been designed for SH2 domain of STAT3, it is necessary to confirm that ODZ10117 does not affect the SH2 domain of other kinase. In addition, it is needed to study whether the STAT3 dimmer is disturbing by the compounds.

In the present study, I demonstrated ODZ10117 effectively suppressed the tyrosine phosphorylation, nuclear translocation, and transcriptional activity of STAT3, resulting in the effective inhibition of migration, invasion, stem cell properties in breast cancer and glioblastoma cells. In addition, ODZ10117 decreased cell viability and induced apoptotic cell death without affecting the proliferation of cancer cells. Finally, the administration of ODZ10117 markedly inhibited tumor growth established in *in vivo* mouse xenograft models of breast cancer and glioma stem cells. However, *in vivo* mouse xenograft models, it is necessary to consider whether the inhibitory effects of tumor growth or epithelial–mesenchymal transition (EMT) is the effect of STAT3 inhibition or the other functions of the ODZ10117. To prove this problem, the mouse xenograft models can be used shSTAT3 transfected cancer cell line.

Although, some of the STAT3 inhibitors, such as Stattic [44] and WP1066 [87] showed more effective inhibition of STAT3 activation than ODZ10117 in the *in vitro* results that were

analyzed from breast cancer cells, hepatocellular carcinoma cells, and glioma cells. Therefore, it is necessary to compare these molecules with ODZ10117. Based on these results, STAT3-targeted therapy should be developed for clinical trials.

In conclusion, this study has shown that ODZ10117 may be a useful candidate for the STAT3-targeted cancer therapy in breast and glioblastoma. ODZ10117 effectively inhibited tyrosine phosphorylation and nuclear translocation of STAT3, resulting in effective anti-tumor activity. These activities included the suppression of migration, invasion, stem cell properties, and tumor growth, induction of apoptotic cell death, and extension of survival rate by targeting STAT3 in both *in vitro* and *in vivo* xenograft models.

REFERENCES

1. Levy, D.E. and C.K. Lee, *What does Stat3 do?* J Clin Invest, 2002. **109**(9): p. 1143-8.
2. Schindler, C. and C. Plumlee, *Inteferons pen the JAK-STAT pathway.* Semin Cell Dev Biol, 2008. **19**(4): p. 311-8.
3. Akira, S., et al., *Molecular cloning of APRF, a novel IFN-stimulated gene factor 3 p91-related transcription factor involved in the gp130-mediated signaling pathway.* Cell, 1994. **77**(1): p. 63-71.
4. Zhong, Z., Z. Wen, and J.E. Darnell, Jr., *Stat3: a STAT family member activated by tyrosine phosphorylation in response to epidermal growth factor and interleukin-6.* Science, 1994. **264**(5155): p. 95-8.
5. Kim, B.H., et al., *Development of Oxadiazole-Based ODZ10117 as a Small-Molecule Inhibitor of STAT3 for Targeted Cancer Therapy.* J Clin Med, 2019. **8**(11).
6. Chen, J., et al., *Inhibition of STAT3 signaling pathway by nitidine chloride suppressed the angiogenesis and growth of human gastric cancer.* Mol Cancer Ther, 2012. **11**(2): p. 277-87.
7. Wang, T., et al., *Regulation of the innate and adaptive immune responses by Stat-3 signaling in tumor cells.* Nat Med, 2004. **10**(1): p. 48-54.
8. Huynh, J., et al., *Therapeutically exploiting STAT3 activity in cancer - using tissue repair as a road map.* Nat Rev Cancer, 2019. **19**(2): p. 82-96.
9. Lee, H., A.J. Jeong, and S.K. Ye, *Highlighted STAT3 as a potential drug target for cancer therapy.* BMB Rep, 2019. **52**(7): p. 415-423.
10. Frank, D.A., *STAT3 as a central mediator of neoplastic cellular transformation.* Cancer Lett, 2007. **251**(2): p. 199-210.
11. Roeser, J.C., S.D. Leach, and F. McAllister, *Emerging strategies for cancer immunoprevention.* Oncogene, 2015. **34**(50): p. 6029-39.
12. Sonnenblick, A., et al., *Tissue microarray-based study of patients with lymph node-positive breast cancer shows tyrosine phosphorylation of signal transducer and activator of transcription 3 (tyrosine705-STAT3) is a marker of good prognosis.* Clin Transl Oncol, 2012. **14**(3): p. 232-6.
13. Schaefer, L.K., et al., *Constitutive activation of Stat3alpha in brain tumors: localization to tumor endothelial cells and activation by the endothelial tyrosine kinase receptor (VEGFR-*

2). Oncogene, 2002. **21**(13): p. 2058-65.
14. Geiger, J.L., J.R. Grandis, and J.E. Bauman, *The STAT3 pathway as a therapeutic target in head and neck cancer: Barriers and innovations.* Oral Oncol, 2016. **56**: p. 84-92.
15. He, G. and M. Karin, *NF-κB and STAT3 - key players in liver inflammation and cancer.* Cell Res, 2011. **21**(1): p. 159-68.
16. Bar-Natan, M., et al., *STAT signaling in the pathogenesis and treatment of myeloid malignancies.* Jakstat, 2012. **1**(2): p. 55-64.
17. Fukuda, A., et al., *Stat3 and MMP7 contribute to pancreatic ductal adenocarcinoma initiation and progression.* Cancer Cell, 2011. **19**(4): p. 441-55.
18. Huynh, J., et al., *Therapeutically exploiting STAT3 activity in cancer — using tissue repair as a road map.* Nature Reviews Cancer, 2019. **19**(2): p. 82-96.
19. Kim, B.-H., E.H. Yi, and S.-K. Ye, *Signal transducer and activator of transcription 3 as a therapeutic target for cancer and the tumor microenvironment.* Archives of Pharmacal Research, 2016. **39**(8): p. 1085-1099.
20. O'Shea, J.J., S.M. Holland, and L.M. Staudt, *JAKs and STATs in immunity, immunodeficiency, and cancer.* N Engl J Med, 2013. **368**(2): p. 161-70.
21. Yu, H., et al., *Revisiting STAT3 signalling in cancer: new and unexpected biological functions.* Nature Reviews Cancer, 2014. **14**(11): p. 736-746.
22. Joyce, J.A. and D.T. Fearon, *T cell exclusion, immune privilege, and the tumor microenvironment.* Science, 2015. **348**(6230): p. 74-80.
23. Spill, F., et al., *Impact of the physical microenvironment on tumor progression and metastasis.* Curr Opin Biotechnol, 2016. **40**: p. 41-48.
24. Herrmann, A., et al., *Targeting Stat3 in the myeloid compartment drastically improves the in vivo antitumor functions of adoptively transferred T cells.* Cancer Res, 2010. **70**(19): p. 7455-64.
25. Kortylewski, M. and H. Yu, *Role of Stat3 in suppressing anti-tumor immunity.* Curr Opin Immunol, 2008. **20**(2): p. 228-33.
26. Groner, B., P. Lucks, and C. Borghouts, *The function of Stat3 in tumor cells and their microenvironment.* Semin Cell Dev Biol, 2008. **19**(4): p. 341-50.
27. Jung, J.E., et al., *STAT3 inhibits the degradation of HIF-1alpha by pVHL-mediated ubiquitination.* Exp Mol Med, 2008. **40**(5): p. 479-85.
28. Samavati, L., et al., *STAT3 tyrosine phosphorylation is critical for interleukin 1 beta and interleukin-6 production in response to lipopolysaccharide and live bacteria.* Mol Immunol, 2009.

46(8-9): p. 1867-77.
29. Gao, H., et al., *Activation of signal transducers and activators of transcription 3 and focal adhesion kinase by stromal cell-derived factor 1 is required for migration of human mesenchymal stem cells in response to tumor cell-conditioned medium.* Stem Cells, 2009. **27**(4): p. 857-65.
30. Fujiwara, Y., M. Takeya, and Y. Komohara, *A novel strategy for inducing the antitumor effects of triterpenoid compounds: blocking the protumoral functions of tumor-associated macrophages via STAT3 inhibition.* Biomed Res Int, 2014. **2014**: p. 348539.
31. Kim, K.J., et al., *STAT3 activation in endothelial cells is important for tumor metastasis via increased cell adhesion molecule expression.* Oncogene, 2017. **36**(39): p. 5445-5459.
32. Sun, X., et al., *Targeting blockage of STAT3 in hepatocellular carcinoma cells augments NK cell functions via reverse hepatocellular carcinoma-induced immune suppression.* Mol Cancer Ther, 2013. **12**(12): p. 2885-96.
33. Debnath, B., S. Xu, and N. Neamati, *Small molecule inhibitors of signal transducer and activator of transcription 3 (Stat3) protein.* J Med Chem, 2012. **55**(15): p. 6645-68.
34. Deng, J., F. Grande, and N. Neamati, *Small molecule inhibitors of Stat3 signaling pathway.* Curr Cancer Drug Targets, 2007. **7**(1): p. 91-107.
35. Pardanani, A., et al., *TG101209, a small molecule JAK2-selective kinase inhibitor potently inhibits myeloproliferative disorder-associated JAK2V617F and MPLW515L/K mutations.* Leukemia, 2007. **21**(8): p. 1658-68.
36. Scuto, A., et al., *The novel JAK inhibitor AZD1480 blocks STAT3 and FGFR3 signaling, resulting in suppression of human myeloma cell growth and survival.* Leukemia, 2011. **25**(3): p. 538-50.
37. Chang, A.Y. and M. Wang, *Molecular mechanisms of action and potential biomarkers of growth inhibition of dasatinib (BMS-354825) on hepatocellular carcinoma cells.* BMC Cancer, 2013. **13**: p. 267.
38. Oyaizu, T., et al., *Src tyrosine kinase inhibition prevents pulmonary ischemia-reperfusion-induced acute lung injury.* Intensive Care Med, 2012. **38**(5): p. 894-905.
39. Gangadhar, T.C., et al., *Phase II study of the Src kinase inhibitor saracatinib (AZD0530) in metastatic melanoma.* Invest New Drugs, 2013. **31**(3): p. 769-73.
40. Aittomäki, S. and M. Pesu, *Therapeutic targeting of the Jak/STAT pathway.* Basic Clin Pharmacol Toxicol, 2014. **114**(1): p. 18-23.
41. Buchert, M., C.J. Burns, and M. Ernst, *Targeting JAK kinase in*

solid tumors: emerging opportunities and challenges. Oncogene, 2016. **35**(8): p. 939-51.
42. Furtek, S.L., et al., *Strategies and Approaches of Targeting STAT3 for Cancer Treatment.* ACS Chem Biol, 2016. **11**(2): p. 308-18.
43. Plimack, E.R., et al., *AZD1480: a phase I study of a novel JAK2 inhibitor in solid tumors.* Oncologist, 2013. **18**(7): p. 819-20.
44. Schust, J., et al., *Stattic: a small-molecule inhibitor of STAT3 activation and dimerization.* Chem Biol, 2006. **13**(11): p. 1235-42.
45. Song, H., et al., *A low-molecular-weight compound discovered through virtual database screening inhibits Stat3 function in breast cancer cells.* Proc Natl Acad Sci U S A, 2005. **102**(13): p. 4700-5.
46. Siddiquee, K., et al., *Selective chemical probe inhibitor of Stat3, identified through structure-based virtual screening, induces antitumor activity.* Proc Natl Acad Sci U S A, 2007. **104**(18): p. 7391-6.
47. Huang, C., et al., *Inhibition of STAT3 activity with AG490 decreases the invasion of human pancreatic cancer cells in vitro.* Cancer Sci, 2006. **97**(12): p. 1417-23.
48. Ferrajoli, A., et al., *WP1066 disrupts Janus kinase-2 and induces caspase-dependent apoptosis in acute myelogenous leukemia cells.* Cancer Res, 2007. **67**(23): p. 11291-9.
49. Siegel, R.L., K.D. Miller, and A. Jemal, *Cancer statistics, 2019.* CA Cancer J Clin, 2019. **69**(1): p. 7-34.
50. Sørlie, T., et al., *Gene expression patterns of breast carcinomas distinguish tumor subclasses with clinical implications.* Proc Natl Acad Sci U S A, 2001. **98**(19): p. 10869-74.
51. Sotiriou, C., et al., *Breast cancer classification and prognosis based on gene expression profiles from a population-based study.* Proc Natl Acad Sci U S A, 2003. **100**(18): p. 10393-8.
52. Bianchini, G., et al., *Triple-negative breast cancer: challenges and opportunities of a heterogeneous disease.* Nat Rev Clin Oncol, 2016. **13**(11): p. 674-690.
53. Dai, X., et al., *Cancer Hallmarks, Biomarkers and Breast Cancer Molecular Subtypes.* J Cancer, 2016. **7**(10): p. 1281-94.
54. Cejalvo, J.M., et al., *Clinical implications of the non-luminal intrinsic subtypes in hormone receptor-positive breast cancer.* Cancer Treat Rev, 2018. **67**: p. 63-70.
55. Davis, M.E., *Glioblastoma: Overview of Disease and Treatment.* Clin J Oncol Nurs, 2016. **20**(5 Suppl): p. S2-8.
56. Shergalis, A., et al., *Current Challenges and Opportunities in Treating Glioblastoma.* Pharmacol Rev, 2018. **70**(3): p. 412-445.
57. Spitzner, M., et al., *STAT3: A Novel Molecular Mediator of*

Resistance to Chemoradiotherapy. Cancers (Basel), 2014. **6**(4): p. 1986-2011.
58. Tan, M.S.Y., et al., *A STAT3-based gene signature stratifies glioma patients for targeted therapy.* Nat Commun, 2019. **10**(1): p. 3601.
59. Becker, S., B. Groner, and C.W. Müller, *Three-dimensional structure of the Stat3beta homodimer bound to DNA.* Nature, 1998. **394**(6689): p. 145-51.
60. Sastry, G.M., et al., *Protein and ligand preparation: parameters, protocols, and influence on virtual screening enrichments.* J Comput Aided Mol Des, 2013. **27**(3): p. 221-34.
61. Chen, I.J. and N. Foloppe, *Drug-like bioactive structures and conformational coverage with the LigPrep/ConfGen suite: comparison to programs MOE and catalyst.* J Chem Inf Model, 2010. **50**(5): p. 822-39.
62. Halgren, T.A., et al., *Glide: a new approach for rapid, accurate docking and scoring. 2. Enrichment factors in database screening.* J Med Chem, 2004. **47**(7): p. 1750-9.
63. Shin, D.S., et al., *Cryptotanshinone inhibits constitutive signal transducer and activator of transcription 3 function through blocking the dimerization in DU145 prostate cancer cells.* Cancer Res, 2009. **69**(1): p. 193-202.
64. Kim, B.H., et al., *A small-molecule compound identified through a cell-based screening inhibits JAK/STAT pathway signaling in human cancer cells.* Mol Cancer Ther, 2008. **7**(9): p. 2672-80.
65. Nelson, E.A., et al., *Nifuroxazide inhibits survival of multiple myeloma cells by directly inhibiting STAT3.* Blood, 2008. **112**(13): p. 5095-102.
66. Li, Y., et al., *Suppression of cancer relapse and metastasis by inhibiting cancer stemness.* Proc Natl Acad Sci U S A, 2015. **112**(6): p. 1839-44.
67. Hu, Y. and G.K. Smyth, *ELDA: extreme limiting dilution analysis for comparing depleted and enriched populations in stem cell and other assays.* J Immunol Methods, 2009. **347**(1-2): p. 70-8.
68. Johnson, D.E., R.A. O'Keefe, and J.R. Grandis, *Targeting the IL-6/JAK/STAT3 signalling axis in cancer.* Nat Rev Clin Oncol, 2018. **15**(4): p. 234-248.
69. Miklossy, G., T.S. Hilliard, and J. Turkson, *Therapeutic modulators of STAT signalling for human diseases.* Nat Rev Drug Discov, 2013. **12**(8): p. 611-29.
70. Clark, A.G. and D.M. Vignjevic, *Modes of cancer cell invasion and the role of the microenvironment.* Curr Opin Cell Biol, 2015. **36**: p. 13-22.
71. Jin, W., *Role of JAK/STAT3 Signaling in the Regulation of Metastasis, the Transition of Cancer Stem Cells, and*

Chemoresistance of Cancer by Epithelial-Mesenchymal Transition. Cells, 2020. **9**(1).
72. *Comprehensive genomic characterization defines human glioblastoma genes and core pathways.* Nature, 2008. **455**(7216): p. 1061-8.
73. Mao, P., et al., *Mesenchymal glioma stem cells are maintained by activated glycolytic metabolism involving aldehyde dehydrogenase 1A3.* Proc Natl Acad Sci U S A, 2013. **110**(21): p. 8644-9.
74. Kim, B.H., et al., *STAT3 Inhibitor ODZ10117 Suppresses Glioblastoma Malignancy and Prolongs Survival in a Glioblastoma Xenograft Model.* Cells, 2020. **9**(3).
75. Hynes, N.E. and W. Gullick, *Therapeutic targeting of signal transduction pathways and proteins in breast cancer.* J Mammary Gland Biol Neoplasia, 2006. **11**(1): p. 1-2.
76. Chai, E.Z., et al., *Targeting transcription factor STAT3 for cancer prevention and therapy.* Pharmacol Ther, 2016. **162**: p. 86-97.
77. Huynh, J., et al., *The JAK/STAT3 axis: A comprehensive drug target for solid malignancies.* Semin Cancer Biol, 2017. **45**: p. 13-22.
78. Baudino, T.A., *Targeted Cancer Therapy: The Next Generation of Cancer Treatment.* Curr Drug Discov Technol, 2015. **12**(1): p. 3-20.
79. Banerjee, K. and H. Resat, *Constitutive activation of STAT3 in breast cancer cells: A review.* Int J Cancer, 2016. **138**(11): p. 2570-8.
80. Sirkisoon, S.R., et al., *Interaction between STAT3 and GLI1/tGLI1 oncogenic transcription factors promotes the aggressiveness of triple-negative breast cancers and HER2-enriched breast cancer.* Oncogene, 2018. **37**(19): p. 2502-2514.
81. Qin, J.J., et al., *STAT3 as a potential therapeutic target in triple negative breast cancer: a systematic review.* J Exp Clin Cancer Res, 2019. **38**(1): p. 195.
82. Rogers, T.W., et al., *The 2016 revision of the WHO Classification of Central Nervous System Tumours: retrospective application to a cohort of diffuse gliomas.* J Neurooncol, 2018. **137**(1): p. 181-189.
83. Hambardzumyan, D. and G. Bergers, *Glioblastoma: Defining Tumor Niches.* Trends in Cancer, 2015. **1**(4): p. 252-265.
84. Piperi, C., K.A. Papavassiliou, and A.G. Papavassiliou, *Pivotal Role of STAT3 in Shaping Glioblastoma Immune Microenvironment.* Cells, 2019. **8**(11).
85. Lin, G.S., et al., *STAT3 Tyr705 phosphorylation affects clinical outcome in patients with newly diagnosed supratentorial glioblastoma.* Med Oncol, 2014. **31**(4): p. 924.

86. Chen, Q., et al., *Targeted inhibition of STAT3 as a potential treatment strategy for atherosclerosis.* Theranostics, 2019. **9**(22): p. 6424-6442.
87. Iwamaru, A., et al., *A novel inhibitor of the STAT3 pathway induces apoptosis in malignant glioma cells both in vitro and in vivo.* Oncogene, 2007. **26**(17): p. 2435-44.

국문 초록

신호변환 및 전사활성인자 3 (STA3)는 많은 종양에서 과발현하고 있으며, 종양 미세 환경에서 STAT3 는 다양한 경로를 통해 지속적으로 활성화되며, 일반적으로 지속적으로 활성화된 STAT3 는 종양의 형성, 진행, 악성도, 재발 및 약물 저항성, 암 줄기세포 특성과 연관되어 있다. 따라서, STAT3 는 암 치료에서 성공 가능성이 매우 높은 단백질로 새로운 종류의 항암제 개발과 암치료에 유망한 표적이다.

이 연구에서 STAT3 의 소분자 억제제로서 3-(2,4-디클로로-페녹시메틸)-5-트리클로로메틸-[1,2,4]옥사디아졸 (ODZ10117)을 발견하였고 이는 STAT3 표적 암치료에 효과적인 치료 효용이 있을 수 있음을 시사하였다. 먼저, ODZ10117 은 다양한 종류의 암, 특히 유방암과 신경교모세포종에서 STAT3 활성화를 효과적으로 억제하는 것을 확인하였으며, 흥미롭게도 다른 STAT 계열 단백질 및 STAT3 상위 신호전달계에 관계없이 STAT3 의 SH2 도메인을 표적으로 하여 STAT3 의 타이로신 인산화, 핵 내로의 이동 및 전사 활성을 억제하는 것을 확인하였다. 또한, STAT3 에 대한 ODZ10117 의 억제 효과는 STAT3 억제제인, S3I-201, STA-21 및 니프록사지드와 같은 잘 알려진 STAT3 억제제 보다 STAT3 의 활성화 저해 능력이 뛰어났다.

ODZ10117 은 암세포의 이동과 침윤을 억제하고, 세포사멸을 유도하였으며, 종양의 성장을 감소시켰다. 이러한 결과를 확인하기 위해, 본 연구에서는 두가지 암 종류에 해당하는 이종 이식 모델을 연구하였다. 첫번째로, 유방암 모델에서 ODZ10117 의 억제 효과는 종양형성을 억제하였으며, 마우스의 생존율을 높이고 폐 전이를 감소시키는 것을 확인하였다. 다음으로, ODZ10117 의 투여는 신경 교

종 줄기세포의 마우스 이종 이식 모델에서도 종양형성을 저해하고 생존율을 높이는 등 치료 효과를 보였다. 결론적으로, 새롭게 발굴한 STAT3 의 소분자 억제 화합물인 ODZ10117 은 종양에서 STAT3 의 활성화 억제를 통해 항암치료에 대한 새로운 치료 전략이 될 수 있음을 시사한다. 나아가, 종양 미세 환경에서 STAT3 의 역할과 종양 미세 환경에서의 ODZ10117 의 새로운 역할을 규명함으로써, 암세포 뿐만 아니라, 종양 미세 환경에서도 STAT3 저해제의 항암작용 역할을 기대할 수 있다.

주요어 : 3-(2,4-디클로로-페녹시메틸)-5-트리클로로메틸-[1,2,4]옥사디아졸 (ODZ10117), 신호변환 및 전사활성인자 3 (STAT3), 표적치료제, 침윤, 세포의 이동, 세포사멸

학 번 : 2012-23672